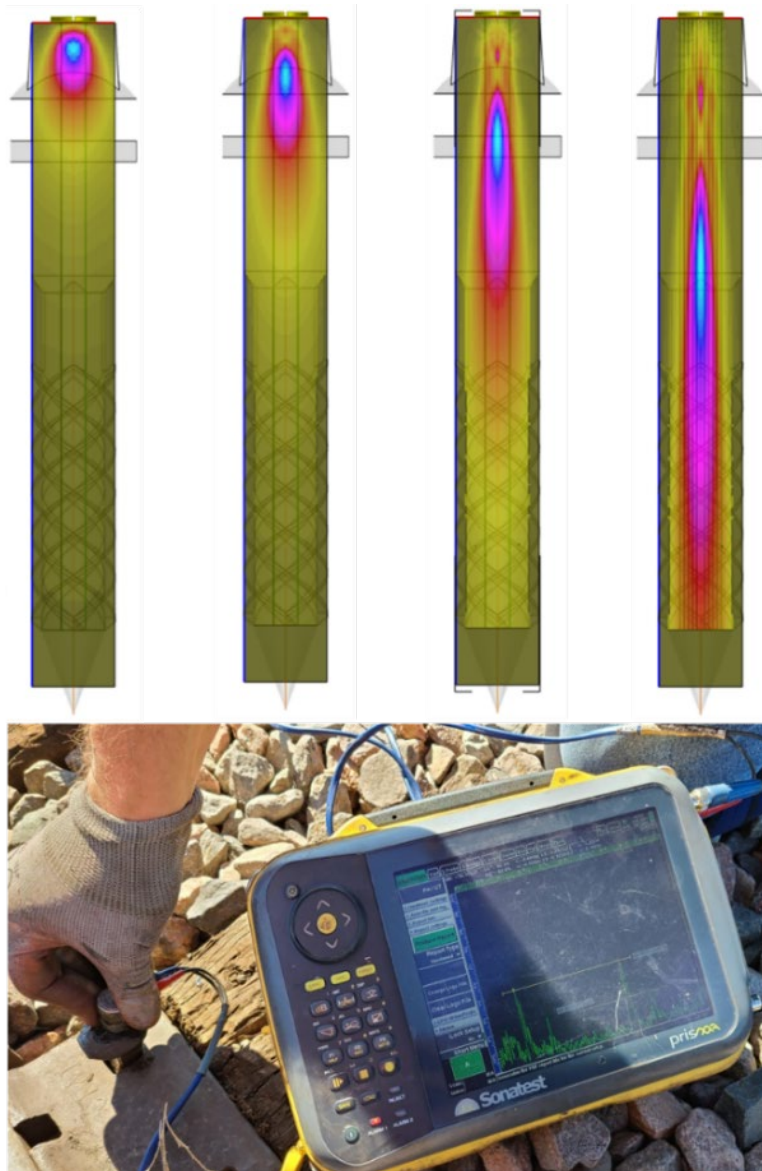




Automated Broken Spike Detection – Phase I



NOTICE

This document is disseminated under the sponsorship of the Department of Transportation in the interest of information exchange. The United States Government assumes no liability for its contents or use thereof. Any opinions, findings and conclusions, or recommendations expressed in this material do not necessarily reflect the views or policies of the United States Government, nor does mention of trade names, commercial products, or organizations imply endorsement by the United States Government. The United States Government assumes no liability for the content or use of the material contained in this document.

NOTICE

The United States Government does not endorse products or manufacturers. Trade or manufacturers' names appear herein solely because they are considered essential to the objective of this report.

REPORT DOCUMENTATION PAGE

Form Approved
OMB No. 0704-0188

The public reporting burden for this collection of information is estimated to average 1 hour per response, including the time for reviewing instructions, searching existing data sources, gathering and maintaining the data needed, and completing and reviewing the collection of information. Send comments regarding this burden estimate or any other aspect of this collection of information, including suggestions for reducing the burden, to Department of Defense, Washington Headquarters Services, Directorate for Information Operations and Reports (0704-0188), 1215 Jefferson Davis Highway, Suite 1204, Arlington, VA 22202-4302. Respondents should be aware that notwithstanding any other provision of law, no person shall be subject to any penalty for failing to comply with a collection of information if it does not display a currently valid OMB control number.

PLEASE DO NOT RETURN YOUR FORM TO THE ABOVE ADDRESS.

1. REPORT DATE (DD-MM-YYYY) 29/09/2020		2. REPORT TYPE Technical Report		3. DATES COVERED (From - To) 09/24/2019-09/30/2020	
4. TITLE AND SUBTITLE Automated Broken Spike Detection – Phase I				5a. CONTRACT NUMBER DTFR5311D00008L	
				5b. GRANT NUMBER	
				5c. PROGRAM ELEMENT NUMBER	
6. AUTHOR(S) Yin Gao – https://orcid.org/0000-0002-5125-5068 Anish Poudel – https://orcid.org/0000-0002-5811-4284 Brian Lindeman – https://orcid.org/0000-0003-3903-266X				5d. PROJECT NUMBER	
				5e. TASK NUMBER Task Order 693JJ619F000104	
				5f. WORK UNIT NUMBER	
7. PERFORMING ORGANIZATION NAME(S) AND ADDRESS(ES) Transportation Technology Center, Inc. 55500 DOT Road, Pueblo, CO 81001				8. PERFORMING ORGANIZATION REPORT NUMBER	
9. SPONSORING/MONITORING AGENCY NAME(S) AND ADDRESS(ES) U.S. Department of Transportation Federal Railroad Administration Office of Railroad Policy and Development Office of Research, Development, and Technology Washington, DC 20590				10. SPONSOR/MONITOR'S ACRONYM(S)	
				11. SPONSOR/MONITOR'S REPORT NUMBER(S) DOT/FRA/ORD-21/17	
12. DISTRIBUTION/AVAILABILITY STATEMENT This document is available to the public through the FRA website .					
13. SUPPLEMENTARY NOTES COR: Cameron Stuart					
14. ABSTRACT Rail spikes connect railroad rails to the supporting crossties and secure tie plates and crossties together. Recent field inspections and observations have revealed broken spike failures (cut spikes and drive/screw spikes) when used with elastic fastener tie plates in mountainous, high-degree curvature territory on North American Class I railroads. Spikes typically break within the crossties, approximately 1 to 1.5 inches below the tie surface, making detection difficult. This study discusses some preliminary efforts to detect the broken spikes using ultrasonic testing (UT) nondestructive evaluation (NDE) approaches. Transportation Technology Center, Inc. performed ultrasonic modeling and simulation to determine and optimize ultrasonic parameters for broken spike detection. Laboratory and in-track testing were also conducted to verify the modeling results and to evaluate the detection accuracy of the UT NDE method. The preliminary results obtained support the continued development of ultrasonic methods for nondestructively, and automatically, detecting broken spikes in track.					
15. SUBJECT TERMS Automated inspection, nondestructive testing, ultrasonic testing, spike breakage					
16. SECURITY CLASSIFICATION OF:			17. LIMITATION OF ABSTRACT	18. NUMBER OF PAGES	19a. NAME OF RESPONSIBLE PERSON Yin Gao, Sr. Engineer
a. REPORT	b. ABSTRACT	c. THIS PAGE			19b. TELEPHONE NUMBER (Include area code)
Unclassified	Unclassified	Unclassified			719-584-0654
			53		

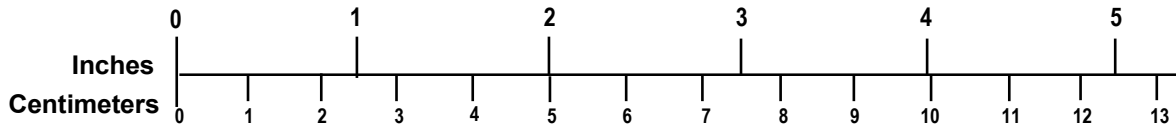
METRIC/ENGLISH CONVERSION FACTORS

ENGLISH TO METRIC

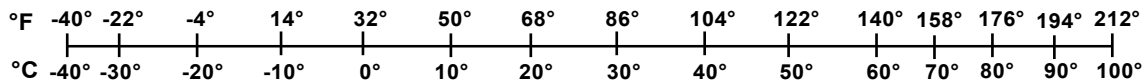
METRIC TO ENGLISH

<p>LENGTH (APPROXIMATE)</p> <p>1 inch (in) = 2.5 centimeters (cm)</p> <p>1 foot (ft) = 30 centimeters (cm)</p> <p>1 yard (yd) = 0.9 meter (m)</p> <p>1 mile (mi) = 1.6 kilometers (km)</p>	<p>LENGTH (APPROXIMATE)</p> <p>1 millimeter (mm) = 0.04 inch (in)</p> <p>1 centimeter (cm) = 0.4 inch (in)</p> <p>1 meter (m) = 3.3 feet (ft)</p> <p>1 meter (m) = 1.1 yards (yd)</p> <p>1 kilometer (km) = 0.6 mile (mi)</p>
<p>AREA (APPROXIMATE)</p> <p>1 square inch (sq in, in²) = 6.5 square centimeters (cm²)</p> <p>1 square foot (sq ft, ft²) = 0.09 square meter (m²)</p> <p>1 square yard (sq yd, yd²) = 0.8 square meter (m²)</p> <p>1 square mile (sq mi, mi²) = 2.6 square kilometers (km²)</p> <p>1 acre = 0.4 hectare (he) = 4,000 square meters (m²)</p>	<p>AREA (APPROXIMATE)</p> <p>1 square centimeter (cm²) = 0.16 square inch (sq in, in²)</p> <p>1 square meter (m²) = 1.2 square yards (sq yd, yd²)</p> <p>1 square kilometer (km²) = 0.4 square mile (sq mi, mi²)</p> <p>10,000 square meters (m²) = 1 hectare (ha) = 2.5 acres</p>
<p>MASS - WEIGHT (APPROXIMATE)</p> <p>1 ounce (oz) = 28 grams (gm)</p> <p>1 pound (lb) = 0.45 kilogram (kg)</p> <p>1 short ton = 2,000 pounds (lb) = 0.9 tonne (t)</p>	<p>MASS - WEIGHT (APPROXIMATE)</p> <p>1 gram (gm) = 0.036 ounce (oz)</p> <p>1 kilogram (kg) = 2.2 pounds (lb)</p> <p>1 tonne (t) = 1,000 kilograms (kg) = 1.1 short tons</p>
<p>VOLUME (APPROXIMATE)</p> <p>1 teaspoon (tsp) = 5 milliliters (ml)</p> <p>1 tablespoon (tbsp) = 15 milliliters (ml)</p> <p>1 fluid ounce (fl oz) = 30 milliliters (ml)</p> <p>1 cup (c) = 0.24 liter (l)</p> <p>1 pint (pt) = 0.47 liter (l)</p> <p>1 quart (qt) = 0.96 liter (l)</p> <p>1 gallon (gal) = 3.8 liters (l)</p> <p>1 cubic foot (cu ft, ft³) = 0.03 cubic meter (m³)</p> <p>1 cubic yard (cu yd, yd³) = 0.76 cubic meter (m³)</p>	<p>VOLUME (APPROXIMATE)</p> <p>1 milliliter (ml) = 0.03 fluid ounce (fl oz)</p> <p>1 liter (l) = 2.1 pints (pt)</p> <p>1 liter (l) = 1.06 quarts (qt)</p> <p>1 liter (l) = 0.26 gallon (gal)</p> <p>1 cubic meter (m³) = 36 cubic feet (cu ft, ft³)</p> <p>1 cubic meter (m³) = 1.3 cubic yards (cu yd, yd³)</p>
<p>TEMPERATURE (EXACT)</p> <p>$[(x-32)(5/9)]^{\circ}\text{F} = y^{\circ}\text{C}$</p>	<p>TEMPERATURE (EXACT)</p> <p>$[(9/5)y + 32]^{\circ}\text{C} = x^{\circ}\text{F}$</p>

QUICK INCH - CENTIMETER LENGTH CONVERSION



QUICK FAHRENHEIT - CELSIUS TEMPERATURE CONVERSION



For more exact and or other conversion factors, see NIST Miscellaneous Publication 286, Units of Weights and Measures. Price \$2.50 SD Catalog No. C13 10286

Updated 6/17/98

Contents

Illustrations	iv
Tables	vi
Executive Summary	vi
1. Introduction	1
1.1 Background	1
1.2 Objectives	2
1.3 Overall Approach	2
1.4 Scope	2
1.5 Organization of the Report	2
2. Ultrasonic Testing Simulations	3
2.1 Ultrasonic Beam Field Modeling and Simulation	3
2.2 Ultrasonic Inspection Simulation	4
2.3 Ultrasonic Modeling and Simulation Parameters	4
2.4 Ultrasonic Beam Field Modeling and Simulation	8
2.5 Summary	21
3. Laboratory Ultrasonic Testing	22
3.1 Electro-discharged Machining Notches	22
3.2 Testing Equipment	23
3.3 Test Procedure	24
3.4 Test Results and Analysis	25
3.5 Discussion of Results	29
4. In-track Ultrasonic Testing	31
4.1 Test Setup	31
4.2 Test Results and Analysis	32
5. Conclusion	35
6. Future Research Recommendations	36
7. References	37
Appendix A: Principles of Ultrasonic Testing and Ultrasonic Transducers	38
Appendix B: Spike Failure Plane Locations	45
Abbreviations and Acronyms	46

Illustrations

Figure 1. (a) Broken cut spikes and (b) broken cut spike within a wood crosstie [1]	1
Figure 2. Schematic showing pencil propagation from a source point on the surface of the active transducer element to two computation points [9].....	3
Figure 3. Ultrasonic inspection simulation step: (a) incident beam on the flaw, (b) ultrasonic beam scattering over the flaw, and (c) echo at reception.....	4
Figure 4. Spikes model used for ultrasonic modeling and simulation: (a) cut spike 2D model and (b) drive spike 3D model	5
Figure 5. Modeled signal in CIVA UT: (a) single-element, 5-MHz, 0-degree transducer and (b) dual-element, 10-MHz, 0-degree transducer	6
Figure 6. Elliptical planar flaw positioning in spikes: (a) cut spike, (b) drive spike	7
Figure 7. Comparison of ultrasonic beam field amplitude along z (propagation) direction for single element transducers in cut spike.....	13
Figure 8. Effect of changing roof angles in the cut spike for 10-MHz transducer: (a) 0 degree, (b) 1 degree, (c) 2 degrees, (d) 3 degrees, and (e) 5 degrees	14
Figure 9. Effect of changing wedge thickness in the cut spike for 10-MHz transducer: (a) 1 mm, (b) 2.5 mm, (c) 5 mm, (d) 7.5 mm, and (e) 10 mm.....	14
Figure 10. Beam field for dual-element, 5-MHz, 0.5-inch transducer in cut spike: (a) 0 degree, (b) 1 degree, (c) 2 degrees, (d) 3 degrees, and (e) 5 degrees	15
Figure 11. Comparison of ultrasonic beam field amplitude along z (propagation) direction for dual-element, 5-MHz, 0.5-inch transducer in the cut spike.....	15
Figure 12. Beam field for dual-element, 10-MHz, 0.5-inch transducer in the cut spike: (a) 0 degree, (b) 1 degree, (c) 2 degrees, (d) 3 degrees, and (e) 5 degrees.....	16
Figure 13. Comparison of ultrasonic beam field amplitude along z (propagation) direction for dual-element, 10-MHz, 0.5-inch transducer in the cut spike	16
Figure 14. Ultrasonic beam field results for 10-MHz, 0.5-inch, dual-element transducer with varying roof angle	21
Figure 15. Comparison of ultrasonic beam field amplitude along z (propagation) direction for dual-element, 10-MHz, 0.5-inch transducer in the drive spike.....	21
Figure 16. Cut spikes with EDM notches	22
Figure 17. Screw spikes with EDM notches.....	22
Figure 18. Ultrasonic flaw detector	23
Figure 19. Transducer on a cut spike	24
Figure 20. A-scan plot of cut spike with 0-degree EDM notch	25
Figure 21. Examples of Broken Spikes.....	27
Figure 22. Spike surface conditions.....	29

Figure 23. Orientation of cut spike failure plane 30
Figure 24. Signal indication by thread layers 34

Tables

Table 1. Ultrasonic and test parameters used for UT beam modeling and simulation	7
Table 2. Comparison of 0-degree, single-element ultrasonic transducers in the cut spike.....	9
Table 3. Comparison of 0-degree, single-element ultrasonic transducers in the cut spike.....	18
Table 4. Dual-element transducer simulation matrix for the drive spike	20
Table 5. Transducers used in laboratory testing	24
Table 6. Laboratory test results.....	28
Table 7. Spike condition for in-track blind test	31
Table 8. In-track test results for cut spikes	32
Table 9. In-track test results for drive spikes.....	32
Table 10 In-track test results for screw spikes.....	33
Table 11. Summary of detection error for in-track testing	33

Executive Summary

Transportation Technology Center, Inc. (TTCI) tested and evaluated an ultrasonic, nondestructive evaluation (NDE) method to detect broken spikes in track through computational modeling, laboratory experiment, and in-track testing. The research detailed in this report was completed between October 2019 and September 2020. This work has led to an improved understanding of what ultrasonic parameters are optimal and how to apply ultrasonic testing (UT) technology to inspect for broken spikes. The findings from this research will be used in future phases to design an in-situ UT inspection procedure for spikes in revenue service.

The overall goal of this research is to develop an automated NDE detection system for spikes. This report summarizes the research and findings of the first phase of this effort which included UT simulation to define the parameters for the ultrasonic inspection, proof-of-concept experimentation, and validation of a conventional hand-held UT NDE method in a controlled environment. UT simulation resulted in recommendations for ultrasonic inspection parameters for broken spike detection. Researchers conducted laboratory testing using various transducers to inspect spikes with both electro-discharged machining (EDM) notches and broken spikes from track to verify the simulation results. They selected three transducers for in-track testing.

Key recommendations resulting from this study are as follows:

- Simulation work showed that the frequency range of 5 MHz to 10 MHz generated good signal reflection at the depth along the spike shaft where in-service spike breaks are typically located. Half-inch diameter transducers were determined to be the best transducer size due to the limitation associated with the contact surface (head of the spike). Dual element transducers with a 0-degree roof angle gave the best signal reflection compared to other dual element transducers with roof angles of 1, 2, 3, and 5 degrees.
- Researchers used seven transducers with various specifications to inspect new spikes, EDM notched spikes, and broken spikes in the laboratory. They evaluated three transducers further during the in-track tests.
- A blind, in-track test, including 10 samples of each spike type (cut spike, drive spike, screw spike), was set up on the High Tonnage Loop at the Facility of Accelerated Testing, Transportation Technology Center. Two transducers gave the best results (clear indication and accurate defect reporting) for the cut spike detection. This finding verified the simulation results, as these two transducers were recommended by the modeling effort. However, none of the transducers were effective in detecting broken drive spikes or screw spikes.
- The orientation of the failure plane and the surface flatness of the spike head can noticeably affect the UT detection. TTCI's survey of cut spikes that failed in service showed that failure planes were typically less than 10 degrees.

Future research will focus on developing a field inspection procedure and investigating potential non-contact detection methods.

1. Introduction

Transportation Technology Center, Inc. (TTCI) tested and evaluated an ultrasonic, nondestructive evaluation (NDE) method to detect broken spikes in track through computational modeling, laboratory experiment, and in-track testing. The research detailed in this report was completed between October 2019 and September 2020. This work has led to an improved understanding of what ultrasonic parameters are optimal and how to apply ultrasonic testing (UT) technology to inspect for broken spikes. The findings from this research will be used in future phases to design an in-situ UT inspection procedure for spikes in revenue service.

1.1 Background

Elastic fastening systems used on railroad wood crossties reduce gage widening and the potential for rail rollover compared to conventional cut spike-only systems. For this reason, elastic fastening systems have been widely installed in high-degree curves on North American Class I railroads. However, recent field inspections and observations have shown a higher frequency of broken spikes (cut spikes and drive/screw spikes) compared to cut spike-only systems when elastic fastener tie plates are installed in locations having steeper grades and curves. [1, 2]

Mechanically, elastic fastening systems behave much differently than cut spike-only systems. Unlike conventional cut spike-only system with rail anchors, tie plates are firmly attached to the rails by the elastic fasteners, allowing the tie plates to move with the rails vertically, laterally, and longitudinally. This load transfer mechanism may allow more wheel-rail forces to be transferred into the spikes compared to cut spike systems. Previous simulation efforts [3-6] have suggested that broken cut spikes are the result of a combined effect of the lateral and longitudinal forces that are transferred into the fastening system. The combined forces can generate stresses on the corner of the spike shaft with high enough amplitude to cause fatigue cracks. Figure 1 shows examples of spike fatigue failures.



Figure 1. (a) Broken cut spikes and (b) broken cut spike within a wood crosstie [1]

Broken spikes are predominately found on the high rail tie plate in curves. Spikes typically break 1 to 1.5 inches below the top surface of the tie (2.5 to 4 inches below the spike head), making the

failures difficult to visually detect. Railroads currently rely on a walking inspection approach to identify broken spikes, tapping the spike with a hammer and distinguishing different sounds (analogous to tap testing) to determine whether a spike is intact or broken. This approach depends solely on the operator's judgement and is qualitative in nature. To date, there is no automated inspection method for identifying broken spikes in track.

1.2 Objectives

The objective of this project was to: 1) investigate whether a UT NDE approach can detect broken spikes, and 2) to develop a practical and effective hand-held UT procedure to detect broken spikes via laboratory and in-track testing.

1.3 Overall Approach

For this first phase of research, TTCI employed a multi-task approach, including ultrasonic beam modeling and simulation in spikes, laboratory testing on individual spikes with artificial defects, and blind UT testing of spikes in track at the High Tonnage Loop (HTL) at the Facility for Accelerated Service Testing (FAST). FAST is a part of the Federal Railroad Administration's Transportation Technology Center near Pueblo, Colorado.

1.4 Scope

The scope of work includes:

- Characterizing and optimizing the ultrasonic inspection parameters using an ultrasonic beam modeling approach.
- Conducting experiments and validating the modeling approach both in the laboratory and on track to investigate and improve the UT inspection procedure.
- Evaluating and analyzing the simulation and test results to recommend appropriate UT parameters for broken spike detection.

1.5 Organization of the Report

This technical report is organized into five primary sections ([Sections 2](#) through [6](#)), along with the associated references ([Section 7](#)) and two appendixes that present the principles of ultrasonic testing and ultrasonic transducers ([Appendix A](#)) and detail the spike failure plane locations ([Appendix B](#)), respectively. [Section 2](#) details the ultrasonic beam modeling and simulation effort to characterize and optimize the ultrasonic parameters for broken spike detection. [Section 3](#) summarizes the laboratory testing, including the preparation of electro-discharged machining (EDM) notches, test procedures, and test results. [Section 4](#) discusses the test setup and results of the in-track blind test using selected transducers based on the laboratory test results. [Section 5](#) summarizes of the efforts presented in this report, and [Section 6](#) offers future recommendations for continued research in the area of broken spike detection.

2. Ultrasonic Testing Simulations

TTCI conducted computer simulations to characterize and optimize the ultrasonic inspection parameters. The UT simulation was conducted for cut spikes and drive spikes using different ultrasonic parameters. The simulation results and recommendations are summarized at the end of the section.

2.1 Ultrasonic Beam Field Modeling and Simulation

The ultrasonic beam field computation was conducted using CIVA UT software. CIVA UT allows users to compute the ultrasonic field of bulk waves radiated by a transducer after refraction through a coupling/test piece interface, or in direct contact with the test piece, for a point or a set of points in the test piece. The ultrasonic wave propagation modeling in CIVA UT is based on the elastodynamic (electromagnetic) wave theory [7]. It relies on an integral formulation of the radiated field and applies the so-called pencil method (a high-frequency approximation) [8] as shown in Figure 2. For this, an ultrasonic transducer is discretized into a series of source points over its surface to calculate the transient wave field in the material.

Some of the assumptions taken into consideration for beam radiation in the coupling medium include [9]:

1. Transducer radiates into the coupling medium.
2. The piezoelectric element vibrates in the thickness mode.
3. No interaction resulting either from cross-talk between elements or from second diffractions from complex radiating surfaces.
4. All source points vibrate with the same time dependence (particle velocity).

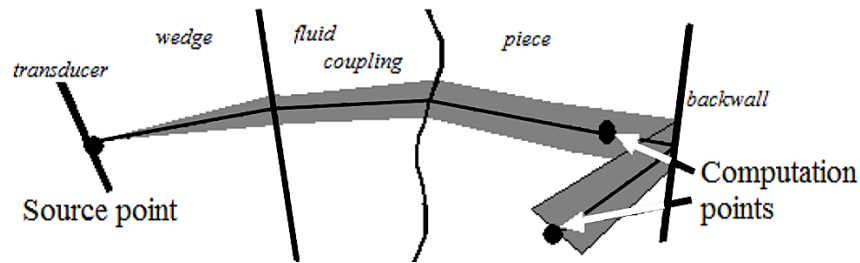


Figure 2. Schematic showing pencil propagation from a source point on the surface of the active transducer element to two computation points [9]

Beam field computation is usually conducted in two stages. The first stage computes various energy paths using Snell's Law. Similarly, in the second stage, the energy associated with each path is quantified by performing the matrix calculations. The vectorial nature of the elastodynamic fields is credited by determining the polarization directions of the various waves according to Christoffel's Law [9]. In addition, the matrix formulation of the pencil method allows a quick estimate of each individual path. The pencil model for prediction of the different elastodynamic quantities relating to the bulk waves (time of flight, amplitude, polarization, and phase of each point source of the probes) originated from a source point to a computation point. In the pencil matrix formulation, the amplitude is related to the divergence of the pencil related to the propagation, as well as wave transmission/reflection coefficients corresponding to each

interaction of the pencil with an interface [10]. Finally, the impulse response is further synthesized from each individual contribution and is convolved with the input signal, as described by the particle displacement relation [10].

$$u(M,t) = V(t) \otimes \iint_{S \in \text{Transducer}} G_M(t) dS \quad (1)$$

where, $G_M(t)$ is the transient Green function evaluated at point M and $V(t)$ is the particle velocity at the transducer surface.

2.2 Ultrasonic Inspection Simulation

The ultrasonic inspection simulation (estimation of the ultrasonic signal received by a probe after attenuation) is conducted in three steps:

1. Computation of the incident beam on the flaw
2. Computation of the ultrasonic beam scattering over the flaw
3. Computation of the received signal using the reciprocity principle [8, 11] to avoid the integration over the probe in reception [12].

Figure 3 demonstrates this ultrasonic inspection simulation process over a simplified steel block with an internal flaw. Different wave scattering theories are applied in CIVA UT and are based solely on the inspection mode (pulse-echo or time-of-flight diffraction ultrasonics) and flaw types considered. Some of these theories include:

1. Kirchhoff
2. Geometrical Theory of Diffraction (GTD)
3. Kirchhoff and GTD
4. Separation of Variables (SOV)
5. Modified Born

Details on these theories can be found in published literature [9, 13].

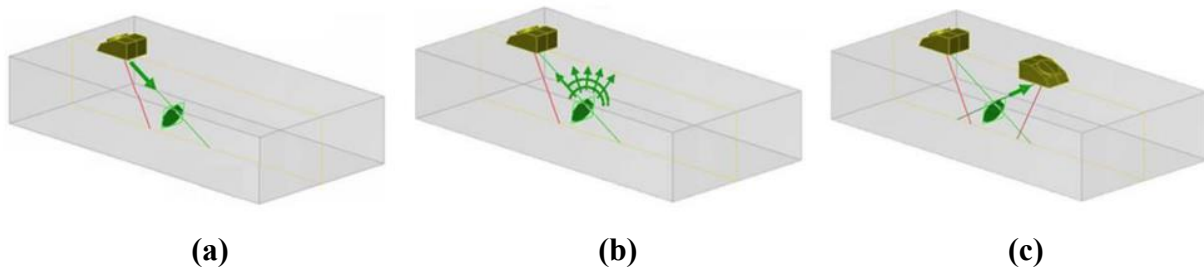
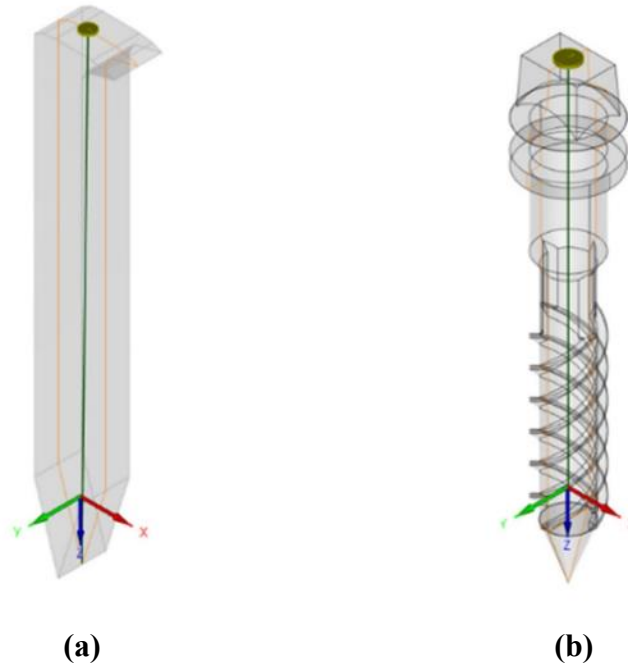


Figure 3. Ultrasonic inspection simulation step: (a) incident beam on the flaw, (b) ultrasonic beam scattering over the flaw, and (c) echo at reception

2.3 Ultrasonic Modeling and Simulation Parameters

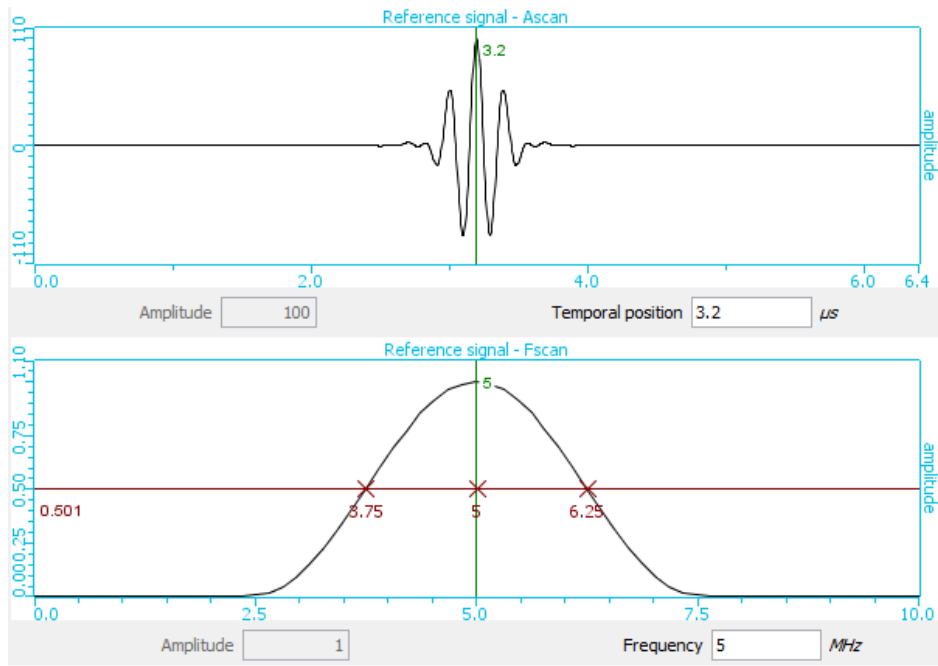
Ultrasonic beam field modeling and simulation for cut spikes and drive spikes with and without flaws were modeled in CIVA UT software. Cut spike ultrasonic simulations used an extruded two-dimensional (2D) CAD profile, but drive spikes simulations used three-dimensional (3D)

SolidWorks® models due to the complex geometry profiles associated with the drive spike. Figure 4 shows the schematic of spikes model chosen to carry out the ultrasonic modeling and simulation.

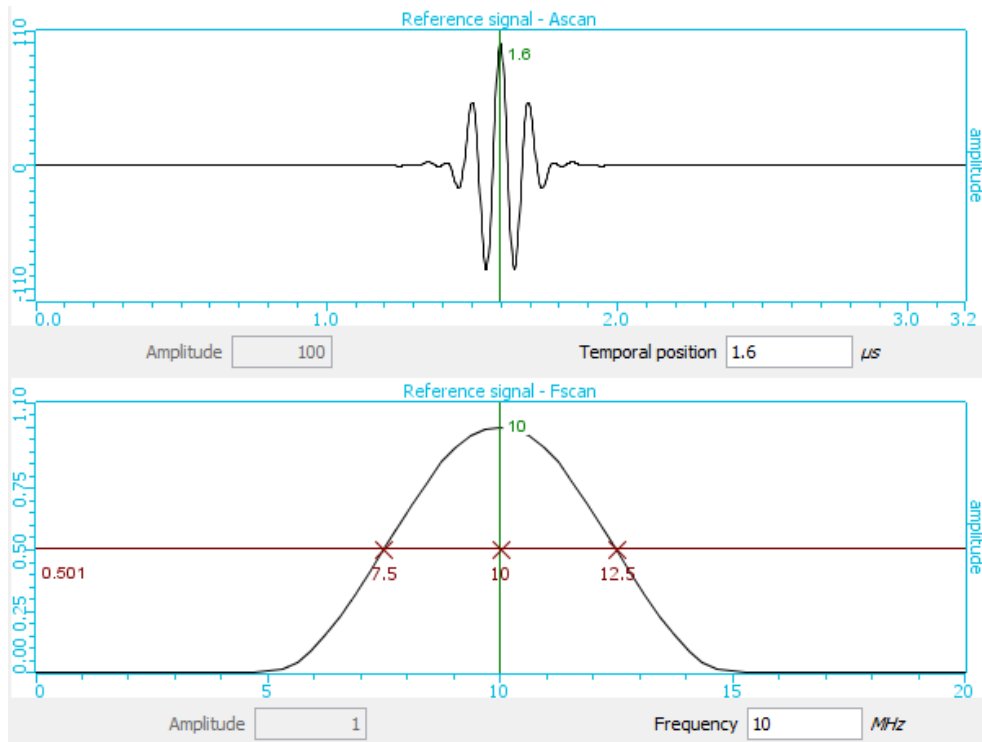


**Figure 4. Spikes model used for ultrasonic modeling and simulation:
(a) cut spike 2D model and (b) drive spike 3D model**

To simulate near-real-world inspection scenarios, ultrasonic parameters chosen must closely match the parameters that are currently available using commercial transducers in the laboratory. Some of the ultrasonic parameters were assumed (probe signal type, bandwidth, phase, number of points and probe positioning, roof angle, and wedge information) for this work. A Hanning window function was applied and a typical 50 percent (-6dB) bandwidth was considered. Figure 5 shows the probe signal modeled for single-element and dual-element transducers. Table 1 shows some of the ultrasonic parameters considered to carry out this modeling and simulation work in CIVA UT.



(a)



(b)

Figure 5. Modeled signal in CIVA UT: (a) single-element, 5-MHz, 0-degree transducer and (b) dual-element, 10-MHz, 0-degree transducer

Table 1. Ultrasonic and test parameters used for UT beam modeling and simulation

UT Simulation Parameters	Cut Spikes		Drive Spikes	
	0 degree	0 degree	0 degree	0 degree
Pattern: single- or dual-element	Single	Dual	Single	Dual
Shape: rectangular or circular	Circular	Half-moon	Circular	Half-moon
Dimension: diameter (in.)	0.25, 0.50.	0.25, 0.50.	0.25, 0.50.	0.25, 0.50, 0.75, 1.0
Apodisation (percent)	0	0	0	0
Focusing Type: flat/cylindrical/spherical	Flat	Flat	Flat	Flat
Wave Type: L-wave or S-wave	L-Wave	L-Wave	L-wave	L-Wave
Probe Type:	Contact	Contact	Contact	Contact
Signal type: Gaussian or Hanning	Hanning	Hanning	Hanning	Hanning
Center Frequency [MHz]	1/2.25/5/10	1/2.25/5/10	1/2.25/5/10	1/2.25/5/10
Bandwidth	50% at -6 dB	50% at -6 dB	50% at -6 dB	50% at -6 dB
Phase (degrees)	0	0	0	0
Sampling Frequency (MHz)	Auto	Auto	Auto	Auto
Number of Points	1,024	1,024	1,024	1,024
Location/Positioning	Center	Center	Center	Center
Offset from the centerline of the spike head (X, Y) (mm)	(2, 9)	(2, 9)	(0, 0)	(0, 0)
Water Path Distance (mm)	N/A	N/A	N/A	N/A
Deflection (degrees)	0	0	0	0
Rotation (degrees)	90	90	90	90
Incidence Angle (degrees)	0	0	0	0
Refracted Angle (degrees)	0	0	0	0

To simulate EDM notches, rectangular and elliptical planar flaws were created in the cut spike and drive spike, respectively. The rectangular flaw was 20 mm × 10 mm (0.78 in. × 0.39 in.) and was positioned to a depth of 76.2 mm (3 in.) for the cut spike. Similarly, the elliptical flaw was 9 mm × 18 mm (0.35 in. × 0.7 in.) and was positioned at the depth of 124 mm (4 in.) for the drive spike (see [Figure 6](#)). These flaw depths were within the range of the common crack depth locations found on spikes. More details of the spike break locations can be found in [Appendix B](#).

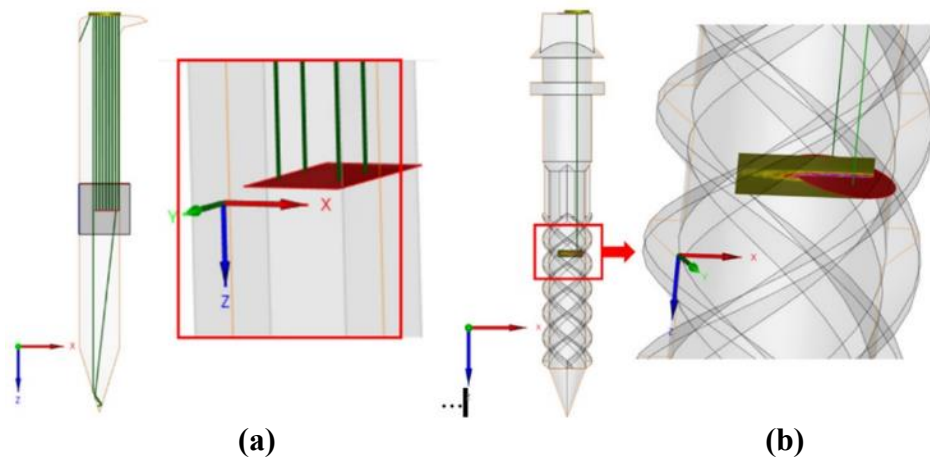


Figure 6. Elliptical planar flaw positioning in spikes: (a) cut spike, (b) drive spike

2.4 Ultrasonic Beam Field Modeling and Simulation

For each ultrasonic probe listed above, ultrasonic beam field computation for longitudinal wave (L-wave) was computed for a cut spike and a drive spike, respectively. This was done to understand the L-wave beam field coverage and response for all ultrasonic probes in both spikes. This section provides beam computation results for each of these scenarios.

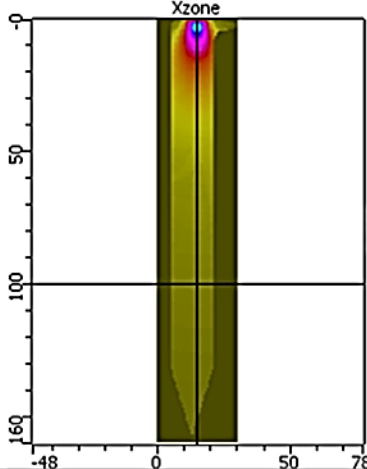
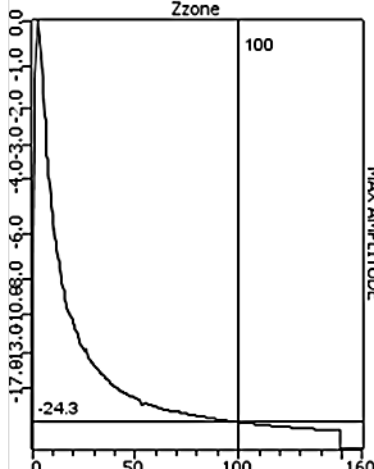
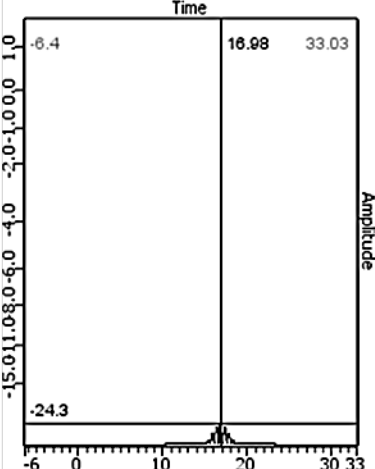
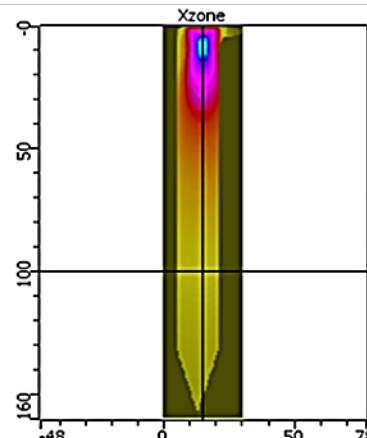
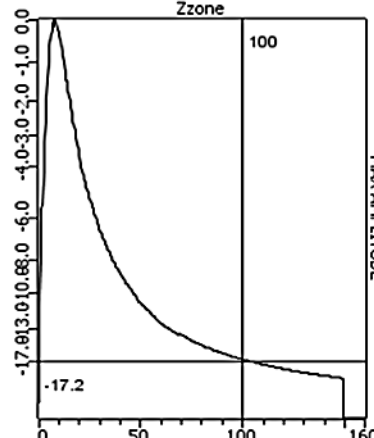
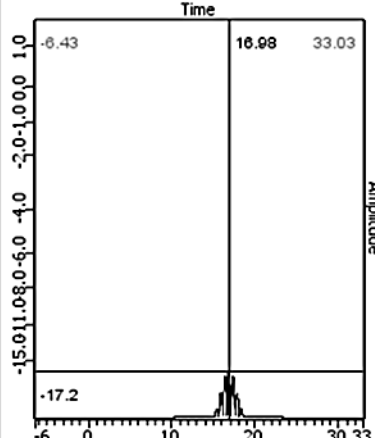
2.4.1 Cut Spike

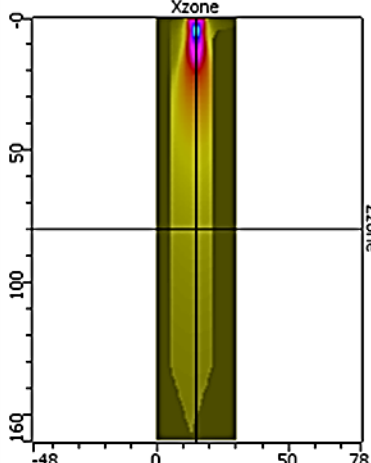
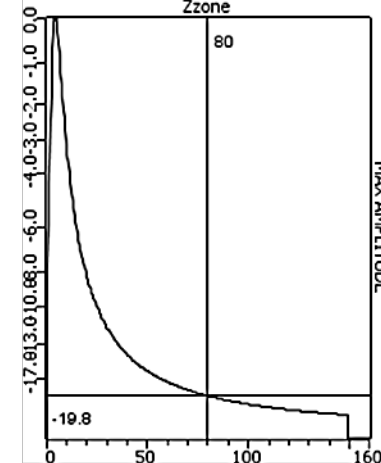
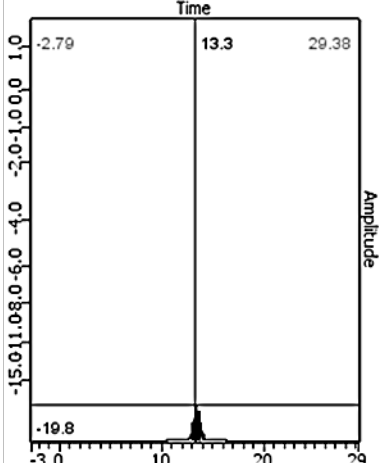
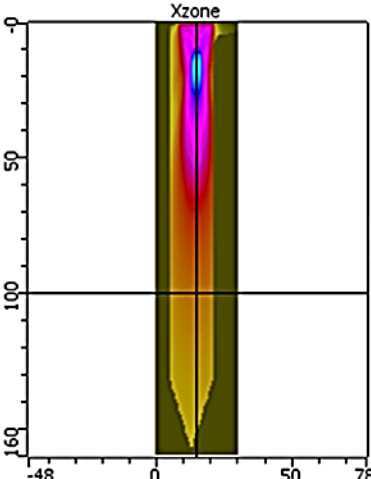
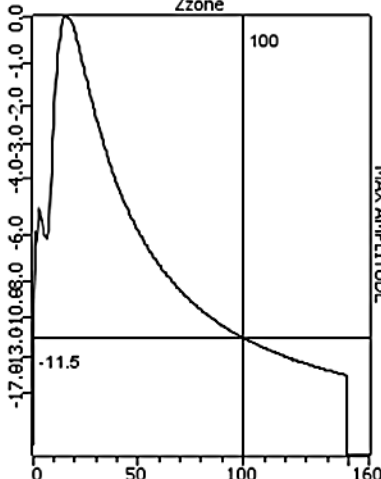
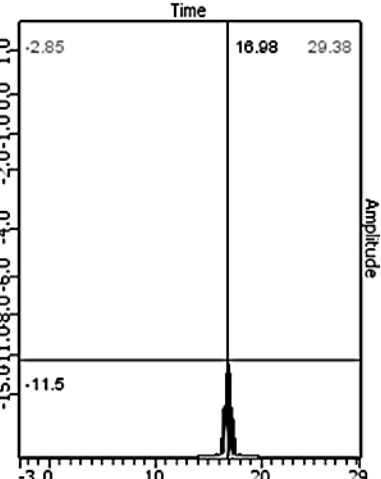
The first part of the study included simulations using single-element transducers. Frequencies of 1 MHz, 2.25 MHz, 5 MHz, and 10 MHz were considered. For each transducer, the element size (diameter of the crystal) used for the simulation was 0.25 inch and 0.5 inch. Element sizes bigger than 0.5 inch were not considered due to the limitation associated with the contact surface of the spike.

[Table 2](#) shows the comparison of the 0-degree, single-element ultrasonic transducer beam field responses in the cut spike. For each transducer type, the first plot shows the ultrasonic beam field in the propagating (z) direction. The second plot shows the maximum signal amplitude in dB at 100-mm deep and the third plot shows the A-scan at a 100-mm depth. An A-scan displays the sound return amplitude and transit time on a simple grid with the vertical axis representing amplitude and the horizontal axis representing time.

The beam field modeling results suggest 5-MHz, 0.5-inch diameter or 10-MHz 0.5-inch diameter single-element transducers provided acceptable coverage at depths up through 100 mm (approximately 4 inches) from the top of the cut spike. This response range covers the area along the spike where cracks are observed, 2.5 inches to 4 inches below the top of the spike head.

Table 2. Comparison of 0-degree, single-element ultrasonic transducers in the cut spike

Transducer Type	2D image beam field	Beam amplitude along z direction	A-scan signal at 100-mm depth
1 MHz, 0.25-inch dia.			
1 MHz, 0.5-inch dia.			

Transducer Type	2D image beam field	Beam amplitude along z direction	A-scan signal at 100-mm depth
<p>2.25 MHz, 0.25-inch dia.</p>			
<p>2.25 MHz, 0.5-inch dia.</p>			

Transducer Type	2D image beam field	Beam amplitude along z direction	A-scan signal at 100-mm depth
<p style="text-align: center;">5 MHz, 0.25-inch dia.</p>			
<p style="text-align: center;">5 MHz, 0.5-inch dia.</p>			

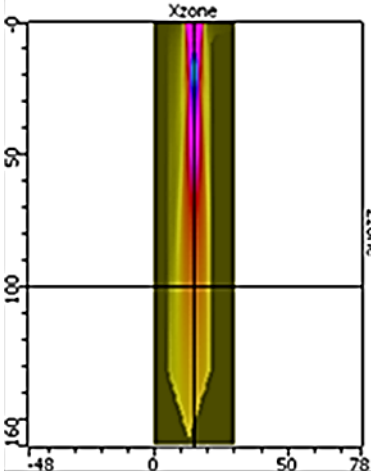
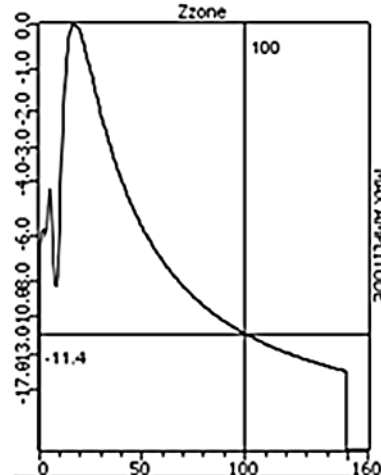
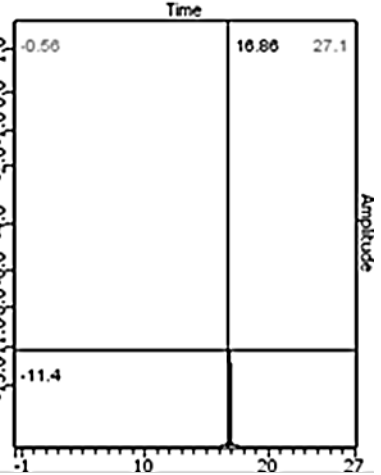
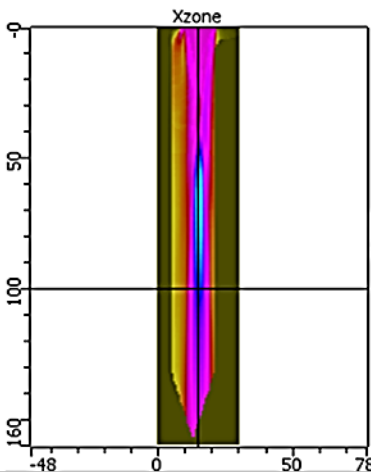
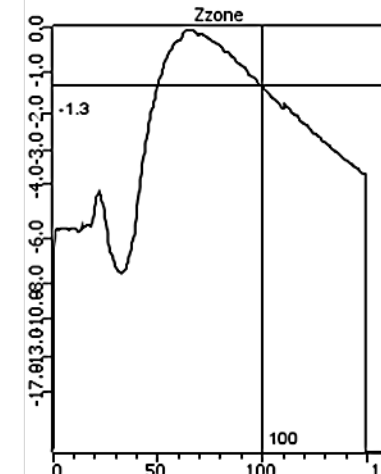
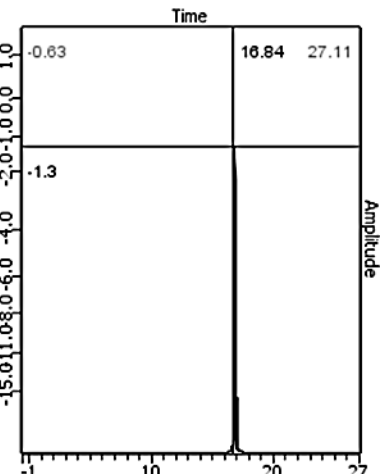
Transducer Type	2D image beam field	Beam amplitude along z direction	A-scan signal at 100-mm depth
<p>10 MHz, 0.25-inch dia.</p>			
<p>10 MHz, 0.5-inch dia.</p>			

Figure 7 shows the comparison plot of the ultrasonic signal amplitude at 100-mm deep (along z direction, propagating direction) for all single-element transducers explored for the cut spike application. Researchers observed that the 0.5-inch, 10-MHz transducer beam amplitude experienced -1.3dB loss and the 0.5-inch, 5-MHz transducer beam experienced a -5.4 dB loss. All other transducers had greater losses.

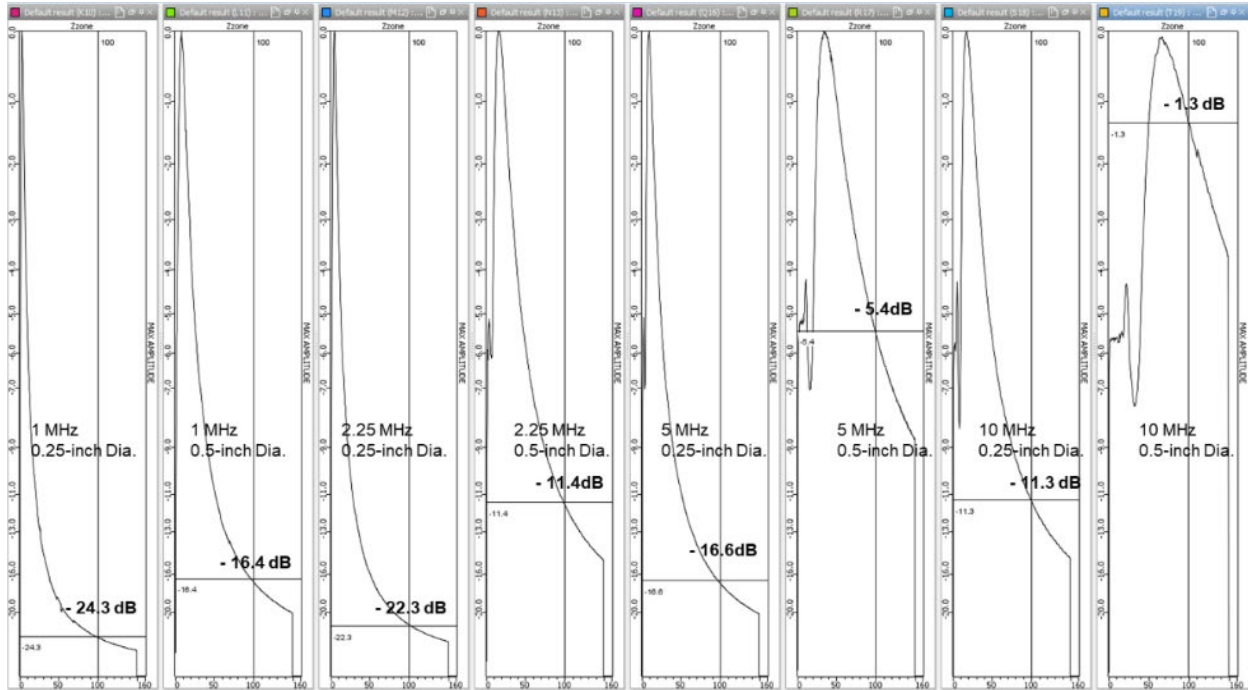


Figure 7. Comparison of ultrasonic beam field amplitude along z (propagation) direction for single element transducers in cut spike

The second part of the simulation focused on using dual-element transducers. For this, only 5-MHz, 0.5-inch and 10-MHz, 0.5-inch dual element transducers were considered. As discussed previously, one of the important parameters associated with the dual-element transducer is the “roof angle,” which is proprietary to each manufacturer. The effect of roof angle was considered as a parameter during the beam field modeling to evaluate likely ranges. This was done to understand the ultrasonic beam coverage using dual-element transducers in the cut spikes. Roof angles of 0, 1, 2, 3, and 5 degrees were considered.

Figure 8 shows the effect of changing the roof angle in the ultrasonic beam field in the spike for the 5-MHz transducer. Researchers demonstrated that by increasing the roof angle, a pseudo-focusing effect was generated that enhanced the near-surface resolution in the focal zone. However, if higher roof angle is used, it is more likely that defects out of the typical zone (1 inch to 1.5 inches below the top of the tie) would be missed.

Next, the wedge or the delay material used for plotting these dual-element transducers were not known. For simulation purposes, Rexolite (L-wave velocity: 2,360 m/s; S-wave velocity: 1,160 m/s) was considered as the wedge or delay material. Also, the spacing between two crystals was set at 2 mm. The thickness of the wedge material was changed from 1 mm to 10 mm and simulations were conducted to see if it would have any significant changes in the beam field of

the dual-element transducer. As shown in Figure 9, changing the wedge thickness had minimal effect in the beam field response of the dual element transducer.

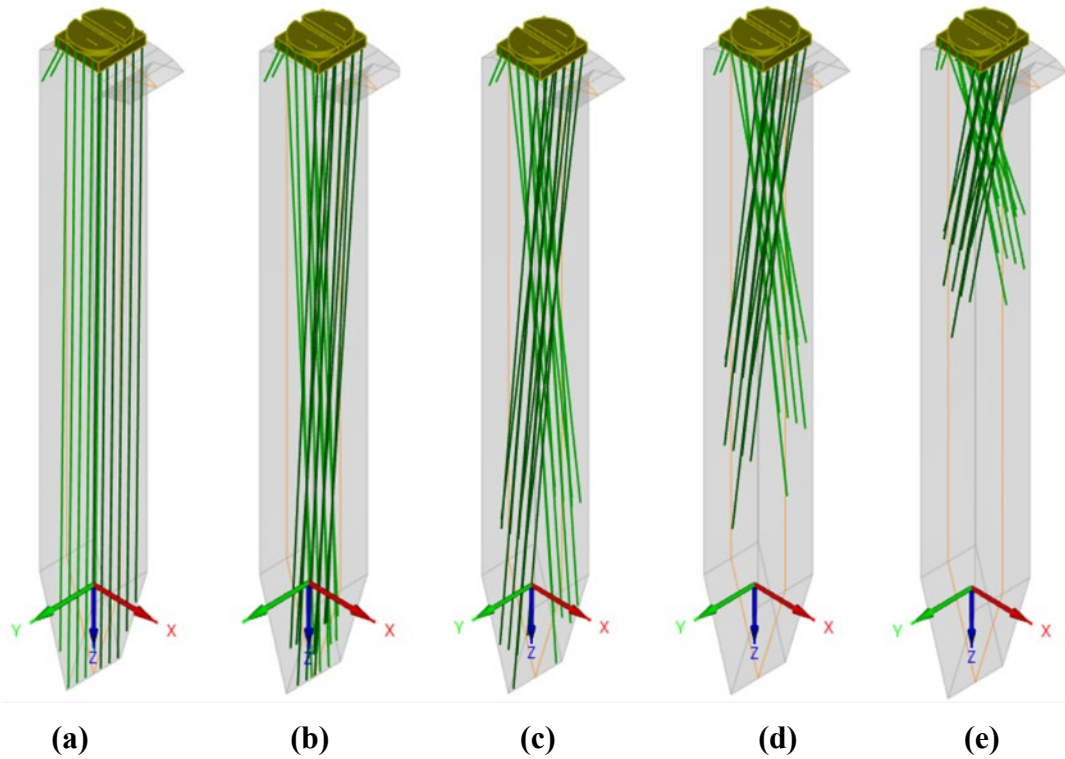


Figure 8. Effect of changing roof angles in the cut spike for 10-MHz transducer: (a) 0 degree, (b) 1 degree, (c) 2 degrees, (d) 3 degrees, and (e) 5 degrees

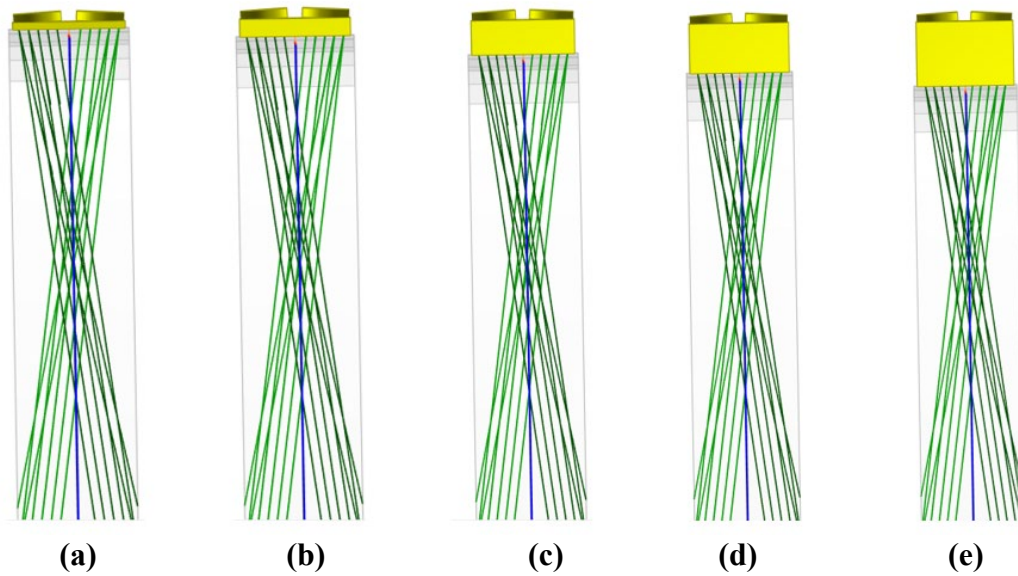


Figure 9. Effect of changing wedge thickness in the cut spike for 10-MHz transducer: (a) 1 mm, (b) 2.5 mm, (c) 5 mm, (d) 7.5 mm, and (e) 10 mm

Figure 10 shows the 0.5-inch, 5-MHz, dual-element ultrasonic transducer beam field responses in the cut spike as a function of roof angle. In each figure, an ultrasonic beam field is shown in the propagating (z) direction. The horizontal line in each figure shows the 100-mm depth from the head of the spike along the propagating direction.

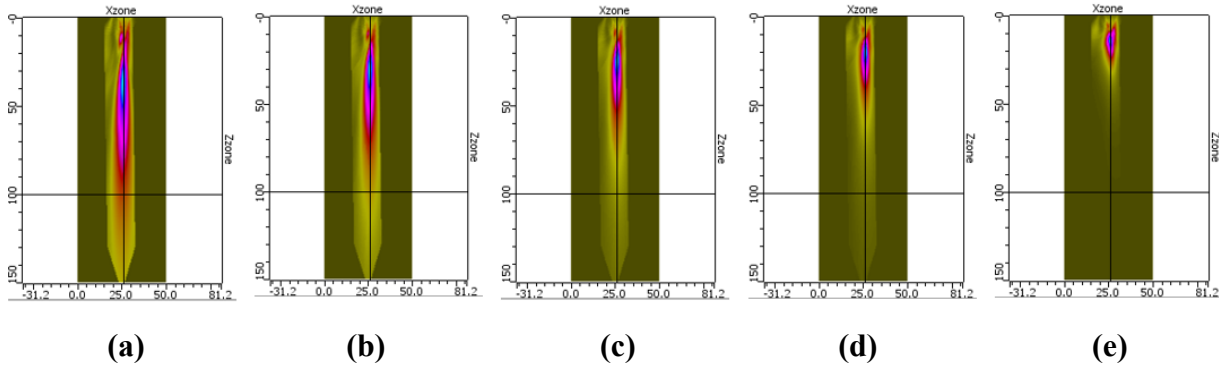


Figure 10. Beam field for dual-element, 5-MHz, 0.5-inch transducer in cut spike: (a) 0 degree, (b) 1 degree, (c) 2 degrees, (d) 3 degrees, and (e) 5 degrees

Similarly, Figure 11 shows the ultrasonic beam field amplitude responses in the cut spike as a function of roof angle for the 0.5-inch, 5-MHz, dual-element transducer. Researchers observed that the beam amplitude decayed exponentially with the increasing roof angle at the 100-mm depth.

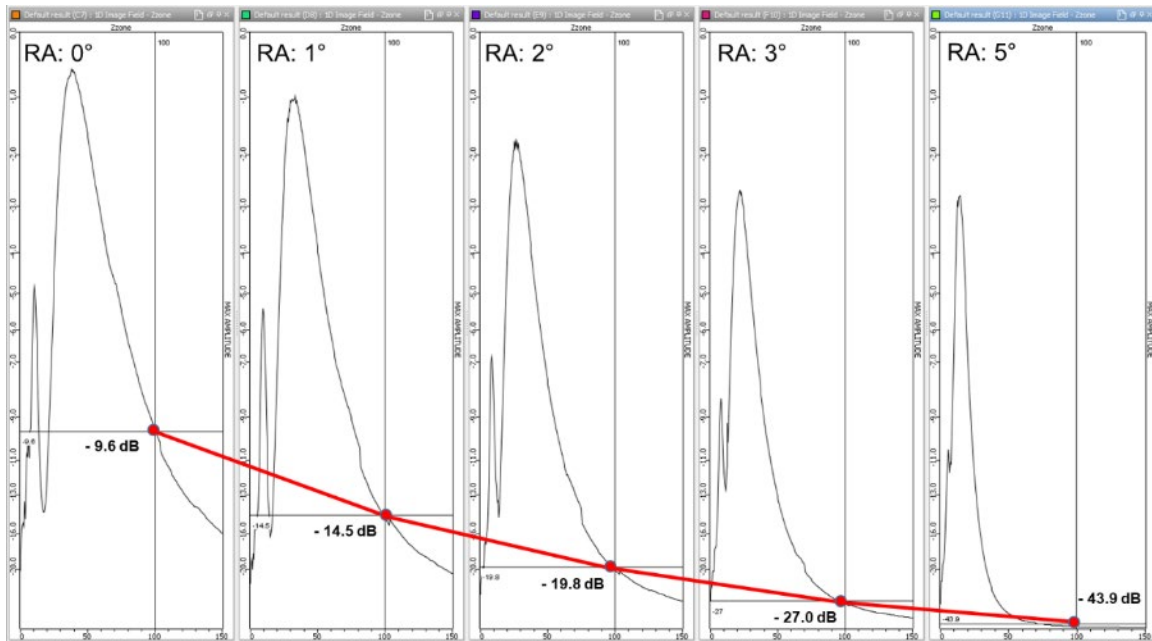


Figure 11. Comparison of ultrasonic beam field amplitude along z (propagation) direction for dual-element, 5-MHz, 0.5-inch transducer in the cut spike

Figure 12 shows the 0.5-inch, 10 MHz, dual-element ultrasonic transducer beam field responses in the cut spike as a function of roof angle. In each figure, an ultrasonic beam field is shown in the propagating (z) direction. The horizontal line in each figure shows the 100-mm depth from the head of the spike along the propagating direction.

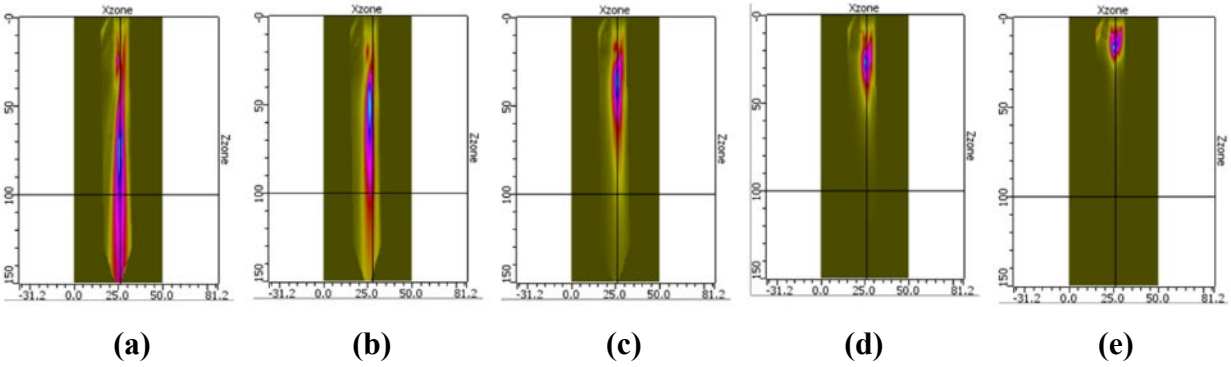


Figure 12. Beam field for dual-element, 10-MHz, 0.5-inch transducer in the cut spike: (a) 0 degree, (b) 1 degree, (c) 2 degrees, (d) 3 degrees, and (e) 5 degrees

Similarly, [Figure 13](#) shows the ultrasonic beam field amplitude responses in the cut spike as a function of roof angle for the 0.5-inch, 10-MHz, dual-element transducer. Researchers observed that the beam amplitude decayed exponentially with the increasing roof angle at the 100-mm depth.

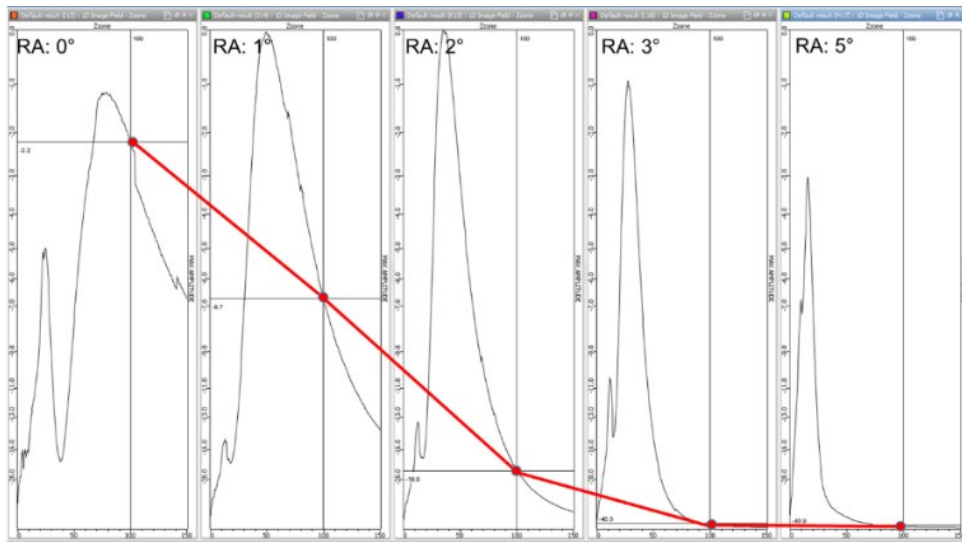


Figure 13. Comparison of ultrasonic beam field amplitude along z (propagation) direction for dual-element, 10-MHz, 0.5-inch transducer in the cut spike

This beam field modeling for dual element transducer suggests using 5-MHz, or 10-MHz, 0.5-inch, dual-element transducers with a 0-degree roof angle, which will provide acceptable coverage at a depth of 100 mm from the top of the cut spike.

2.4.2 Drive Spike

Like the cut spike simulation, the first part of the study for the drive spike included simulations using single-element transducers with a variety of frequencies (1 MHz, 2.25 MHz, 5 MHz, and 10 MHz). Since the 0.25-inch transducer did not provide acceptable signal coverage for the cut spike simulation, the element size (diameter of the crystal) considered for the drive spike simulation was limited to the 0.5-inch model. Due to the limitations associated with the contact surface (head of the spike), sizes greater than 0.5 inch were not considered. [Table 3](#) shows the

comparison of the 0-degree, single-element, ultrasonic transducer beam field responses. Similarly, for each transducer type, the first plot shows the ultrasonic beam field in the propagating (z) direction. The second plot shows the maximum signal amplitude in dB at 100-mm deep, and the third plot shows the A-scan at a 100-mm depth.

The beam field modeling results presented for the drive spike suggests 5-Hz, 0.5-inch diameter or 10-MHz, 0.5-inch diameter single-element transducers provided adequate coverage at a depth of 100 mm from the top of the drive spike.

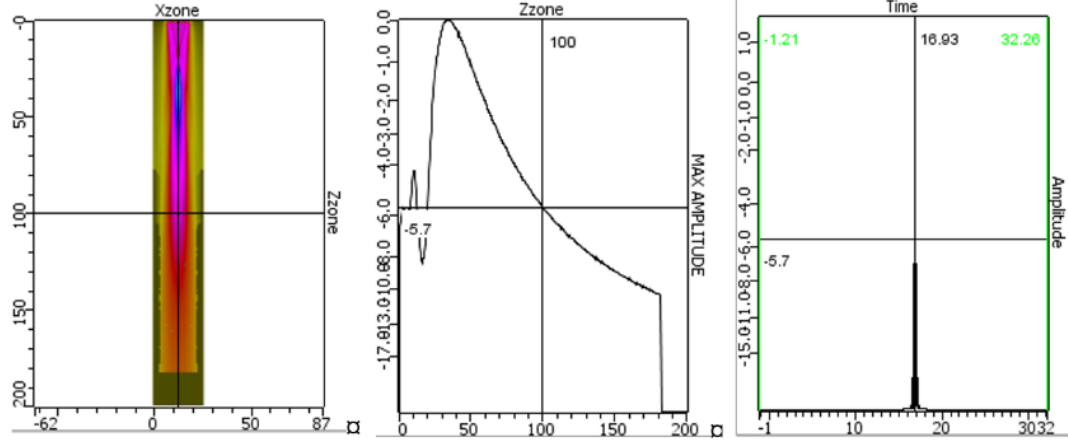
As in the cut spike simulation, the second part of the simulation focused on dual-element transducers. Several simulations were conducted to determine the correct dual-element transducer configuration. [Table 4](#) shows the simulation matrix. For simulation purposes, Rexolite (L-wave velocity: 2,360 m/s; S-wave velocity: 1,160 m/s) was considered as the wedge or the delay material. In addition, the spacing between crystals was set at 1 mm and the thickness of the wedge material considered was 1 mm.

A red “x” in the table indicates there was inadequate signal for that particular probe configuration, whereas the blue shaded boxes suggest good signal response for that probe configuration at about 100 mm deep.

Table 3. Comparison of 0-degree, single-element ultrasonic transducers in the cut spike

Transducer Type	2D image beam field	Beam amplitude along z direction	A-scan signal at 100-mm depth
<p>1 MHz, 0.5-inch dia.</p>			
<p>2.25 MHz, 0.5-inch dia.</p>			

5 MHz, 0.5-inch dia.



10 MHz, 0.5-inch dia.

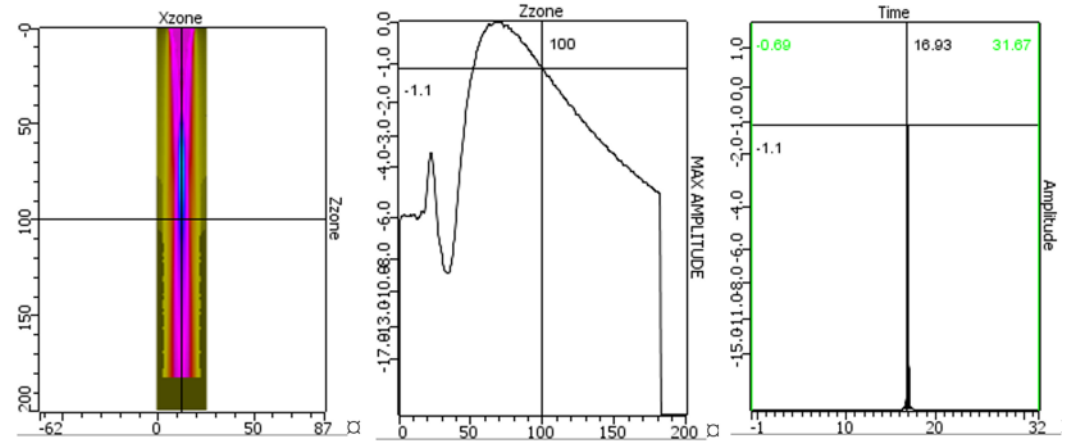


Table 4. Dual-element transducer simulation matrix for the drive spike

Transducer Frequency	Transducer Diameter	Roof Angle					
		0°	1°	2°	3°	4°	5°
2.25 MHz	6.35 mm	x	x	x	x	x	x
	12.7 mm	x	x	x	x	x	x
	19.05 mm	x	x	x	x	x	x
	25.4 mm	x	x	x	x	x	x
4.5 MHz	6.35 mm	x	x	x	x	x	x
	12.7 mm	x	x	x	x	x	x
	19.05 mm	✓	✓	x	x	x	x
	25.4 mm	✓	✓	x	x	x	x
6.75 MHz	6.35 mm	x	x	x	x	x	x
	12.7 mm	x	x	x	x	x	x
	19.05 mm	✓	✓	x	x	x	x
	25.4 mm	✓	✓	x	x	x	x
9 MHz	6.35 mm	x	x	x	x	x	x
	12.7 mm	✓	✓	x	x	x	x
	19.05 mm	✓	✓	✓	x	x	x
	25.4 mm	✓	✓	✓	x	x	x
11.25 MHz	6.35 mm	x	x	x	x	x	x
	12.7 mm	✓	✓	x	x	x	x
	19.05 mm	✓	✓	x	x	x	x
	25.4 mm	✓	✓	x	x	x	x

Beam field modeling results for the drive spike suggests using a higher-frequency transducer with a crystal diameter of at least 0.5-inch to achieve acceptable beam coverage and signal amplitude at a depth of 100 mm from the top of the drive spike. [Figure 14](#) shows the ultrasonic beam computation results for different roof angles defined for the 10-MHz, 0.5-inch, dual-element transducer. [Figure 15](#) presents the signal amplitude at 100 mm depth from the top of the drive spike. It shows that a 0-degree roof angle generated the best signal at the depth of interest.

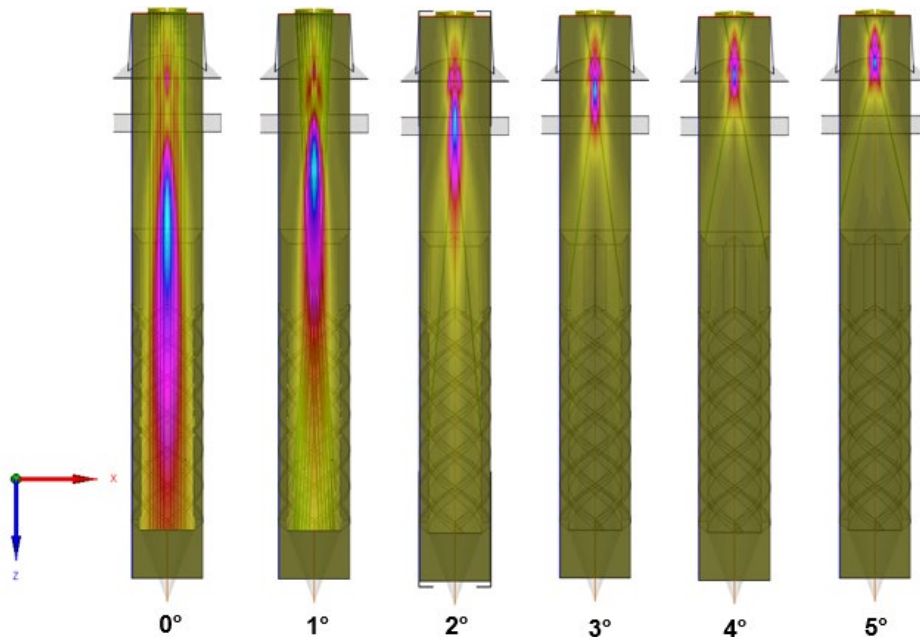


Figure 14. Ultrasonic beam field results for 10-MHz, 0.5-inch, dual-element transducer with varying roof angle

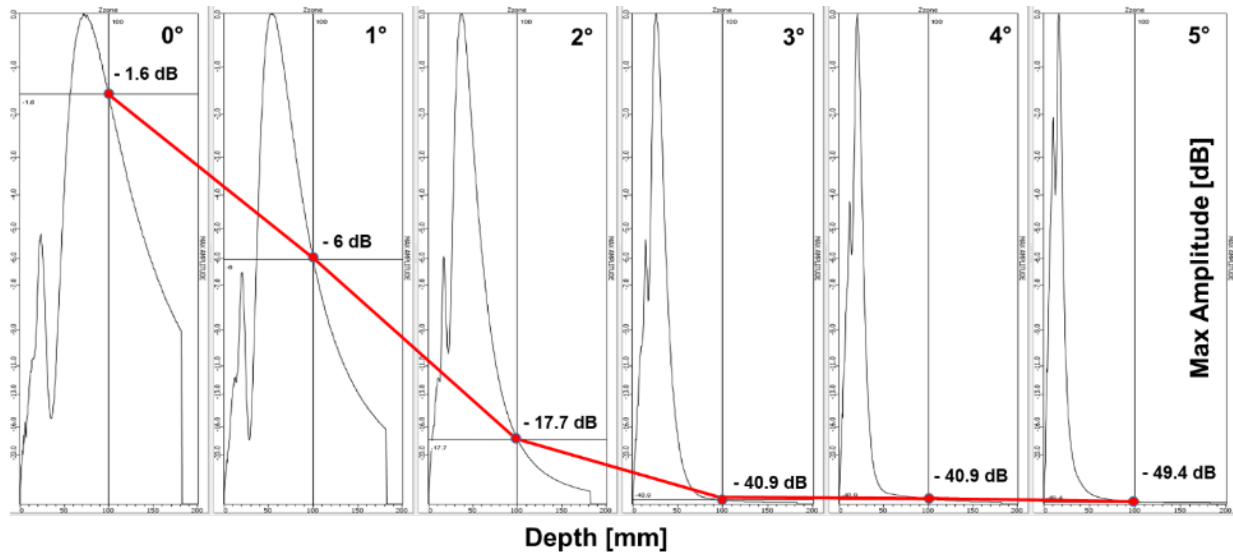


Figure 15. Comparison of ultrasonic beam field amplitude along z (propagation) direction for dual-element, 10-MHz, 0.5-inch transducer in the drive spike

2.5 Summary

This section first introduced the principle of ultrasonic testing and ultrasonic transducers to better understand the test results. The UT simulation was conducted for cut spikes and drive spikes. Different ultrasonic parameters, transducer frequencies, transducer sizes, and roof angles of dual-element transducers were evaluated in the simulation. The simulation goals were to characterize and optimize the ultrasonic inspection parameters. Based on the simulation results, key findings are as follows:

- The 0.5-inch, 5-MHz to 10-MHz transducers generated acceptable ultrasonic beam responses at the desired depth (where cracks typically locate on the spike shaft).
- The 0.5-inch diameter transducer was considered the largest practical size given the size of the contact surface area on the head of a spike.
- A 0-degree roof angle is also recommended for dual-element transducers.

3. Laboratory Ultrasonic Testing

Leveraging the simulation results, TTCI conducted laboratory testing of the transducers to evaluate their effectiveness in detecting breaks in actual spikes. First, spike samples with electro-discharged machining (EDM) notches were fabricated for controlled laboratory tests. Second, a hand-held UT procedure was developed and tests conducted to test spikes (cut spikes, drive spikes, and screw spikes) with EDM notches and broken spikes from the track. The laboratory testing was performed to aid in understanding UT signal responses for defective spikes and for comparison to the baseline measurements (new spikes).

3.1 Electro-discharged Machining Notches

EDM notches were made on three cut spikes and three screw spikes with different orientations of the cutting planes. These EDM notches were created 3 inches below the top of the cut spike head and screw spike head. The location of the notches was determined based on the breakage location of spikes that failed in service. The main reason for the EDM notched spikes was to provide controlled defects (known locations and orientations) to evaluate the effectiveness of different transducers.

The cutting planes were oriented at 0, 10, and 20 degrees relative to the horizontal plane. The notches were cut halfway through the cross-section of the spike shaft. The width of these notches was 5 mils (0.005 in.). These tight EDM notches were created to simulate a tight crack and were tested during the UT calibration process. Figures 16 and 17 show drawings and photos of actual spikes with EDM notches.

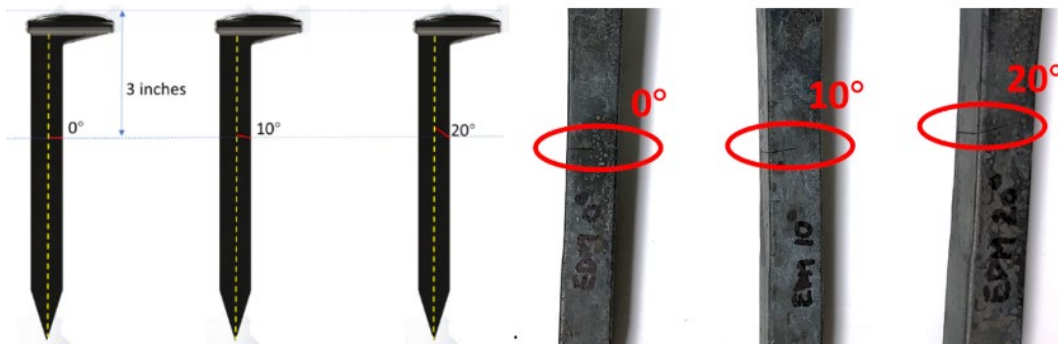


Figure 16. Cut spikes with EDM notches

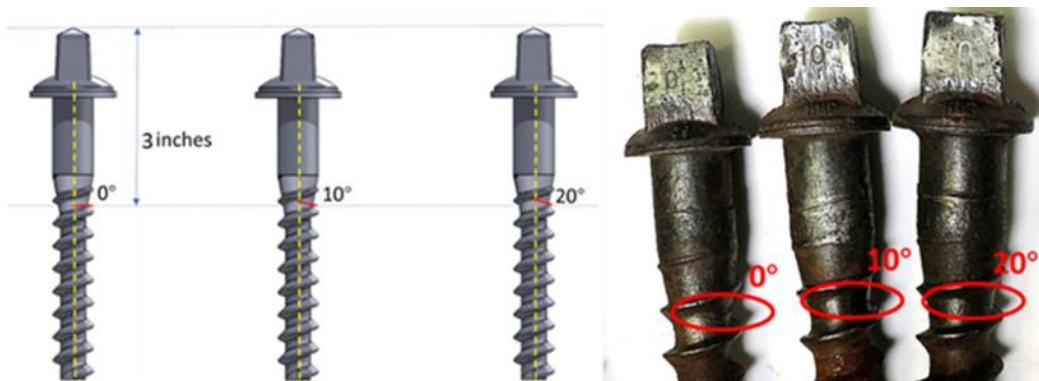


Figure 17. Screw spikes with EDM notches

3.2 Testing Equipment

An Olympus EPOCH 650 ultrasonic flaw detector was used for laboratory and in-track testing (Figure 18). Transducers are connected to the flaw detector for broken spike detection. The detector generates amplitude scans (A-scans) for defect identification. The magnitude of signal amplitude indicates whether there is a flaw present in a spike (spike breakage, in this study). A distinct amplitude at the depth of interest indicates spike breakage.



Figure 18. Ultrasonic flaw detector
Photo credit: Olympus Corporation

Researchers used a total of seven transducers in laboratory testing. The transducers included various transducer diameters, frequencies, and types (single- or dual-element) as presented in [Table 5](#).

Based on the modeling results, Transducers 4 and 5 were recommended for broken spike detection. The others were included in the test for comparison of the effectiveness of different transducers and were also considered as a part of the simulation verification. All the dual-element transducers in Table 4 were 0-degree roof angle transducers.

Table 5. Transducers used in laboratory testing

Transducer Number	1	2	3	4	5	6	7
Transducer Diameter Size	0.5-inch	0.5-inch	0.25-inch	0.5-inch	.5-inch	0.283-inch	0.25-inch
Transducer Element Shape	Circular	Circular	Circular	Circular	Circular	Circular	Circular
Transducer Frequency	1.0 MHz	2.25 MHz	2.25 MHz	5 MHz	5.0 MHz	7.5 MHz	10.0 MHz
Transducer Element Type	Single	Single	Single	Single	Dual	Dual	Dual

3.3 Test Procedure

The test procedure developed was the same for all types of spikes tested. The spikes were supported vertically and the transducer was placed on the head directly over the spike's shaft, as shown in [Figure 19](#). A water-based ultrasonic couplant (SoniX™ from ECHO Ultrasonics) was used for the testing.



Figure 19. Transducer on a cut spike

[Figure 20](#) shows the A-scan results of the cut spike with 0-degree EDM notch using a 0.5-inch diameter, 5-MHz, dual-element transducer. The x-axis is the position along the spike from the spike head; y-axis is the signal amplitude, ranging from 0 percent to 100 percent of the full screen height. The signal had several relatively high amplitude peaks near the spike head (0 to 1 in.) and at 3 inches below the spike head. The high amplitude at the spike head might have been caused by signal reflection due to the uneven contact surface between the transducer and spike head. This is not the depth of interest along the spike shaft since the spike breakage typically does not occur in this region. The signal amplitude in the range of 2.5 to 4 inches below the top of spike head is important since this is the area where the spike breakage is commonly found in the field. A signal with high amplitude at 3 inches was clearly displayed in the A-scan plot ([Figure 20](#)), indicating that the flaw was successfully detected.

Drive spikes and screw spikes were tested using the same test procedure. The test results for different spikes and different transducers are summarized in the next section.

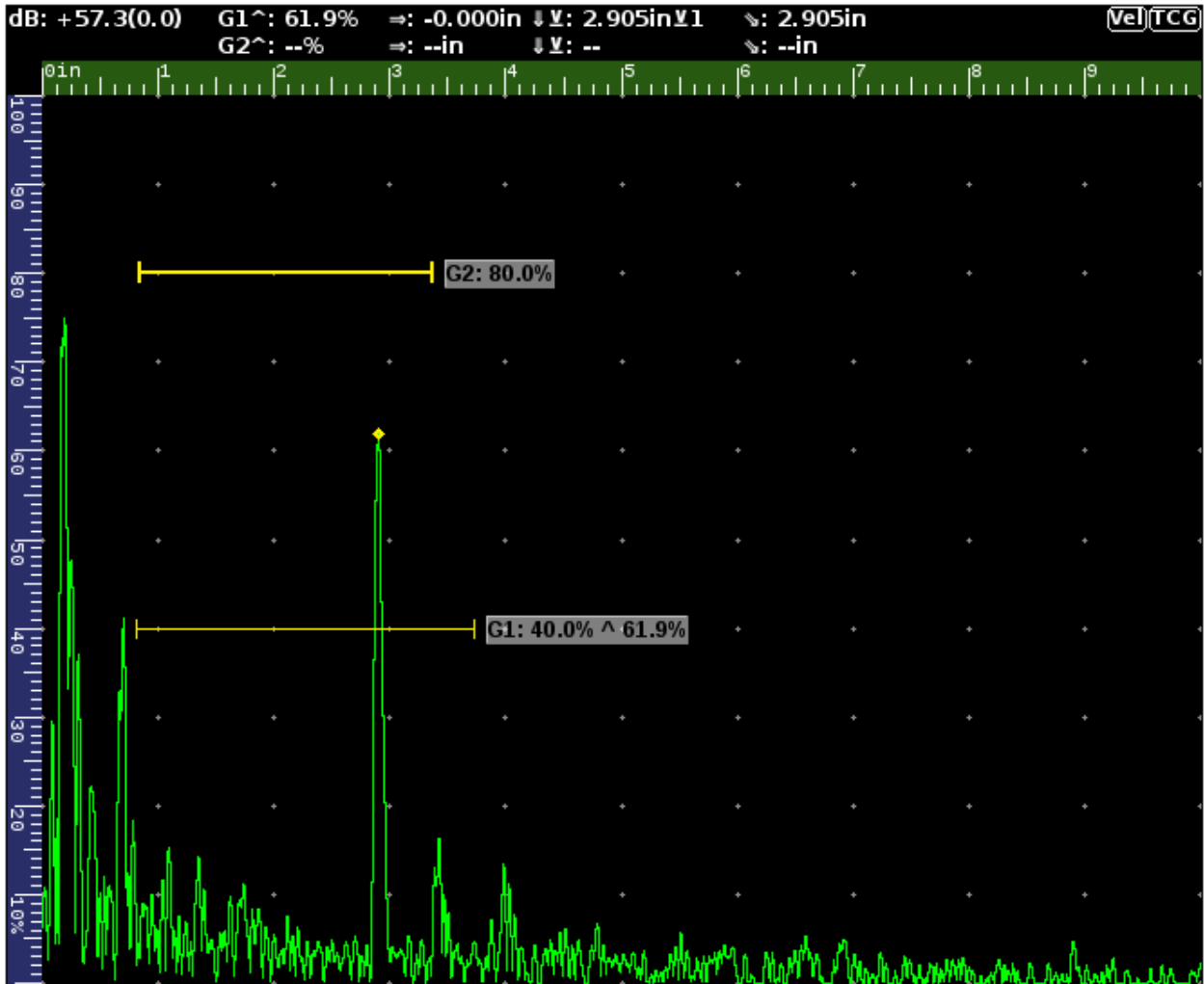


Figure 20. A-scan plot of cut spike with 0-degree EDM notch

3.4 Test Results and Analysis

Table 6 provides laboratory test results. For each type of spike (cut spike, screw spike, and drive spike), a new spike and three broken spikes that failed in service were included in the test. The spikes were fully broken (Figure 21). The spikes with EDM notches were also included in this test. The percentage of signal amplitude was documented for each test case. The higher the signal amplitude, the better the indication of the defect. The laboratory testing shows the following key findings:

- New spikes: All transducers correctly measured no breakage in the new spikes.
- For the spikes that failed in service:
 - Transducer 5 generated 100 percent of signal amplitude for cut spikes and drive spikes and clearly indicated the defects in screw spikes.

- Transducers 2 and 4 clearly indicated broken spikes, but the indication was not as strong as Transducer 5. All signal amplitude percentages were above 36 percent (except one no indication for Transducer 2).
- Transducers 6 and 7 could indicate broken spikes, but most of the signal amplitude percent was below 25 percent (except for cut spike detection using transducer 7).
- Transducers 1 and 3 did not show any indication.
- For the detection of EDM-notched spikes:
 - Generally, the signal amplitude percent decreased as the orientation angle increased.
 - Transducer 2 generated the best indication for screw spikes, and Transducer 5 generated the best indication for cut spikes.

The preliminary laboratory test showed that a defect could be located in a spike. Transducers 2, 4, and 5 were selected for in-track testing.



(a) Cut spikes



(b) Drive spikes



(c) Screw spikes

Figure 21. Examples of Broken Spikes

Table 6. Laboratory test results

Transducer Number	1	2	3	4	5	6	7
Transducer Diameter Size	0.5 inch	0.5 inch	0.25 inch	0.5 inch	.5 inch	.283 inch	.25 inch
Transducer Frequency	1.0 MHz	2.25 MHz	2.25 MHz	5 MHz	5.0 MHz	7.5 MHz	10.0 MHz
Transducer Type	Single	Single	Single	Single	Dual	Dual	Dual
	↓	↓	↓	↓	↓	↓	↓
Spike Condition	Indication	Indication	Indication	Indication	Indication	Indication	Indication
Cut Spike - New	No indication	No indication	No indication	No indication	No indication	No indication	No indication
Cut Spike - Broken	No indication	38%	No indication	47%	100%	19%	55%
Cut Spike –Broken	No indication	No indication	No indication	40%	100%	12%	34%
Cut Spike - Broken	No indication	90%	No indication	80%	100%	25%	40%
Cut Spike - 0° EDM	No indication	46%	No indication	46%	62%	10%	49.7%
Cut Spike - 10° EDM	No indication	No indication	No indication	23%	17%	5%	No indication
Cut Spike - 20° EDM	No indication	No indication	No indication	12%	16%	No indication	No indication
Screw Spike - New	No indication	No indication	No indication	No indication	No indication	No indication	No indication
Screw Spike - Broken	No indication	68%	No indication	45%	100%	14%	12%
Screw Spike - Broken	No indication	100%	No indication	36%	54%	10%	8%
Screw Spike - Broken	No indication	52%	No indication	76%	56%	8%	No indication
Screw Spike - 0° EDM	No indication	100%	No indication	46%	12%	12.7%	No indication
Screw Spike - 10° EDM	No indication	41%	No indication	11%	33%	9.4%	25.0%
Screw Spike - 20° EDM	No indication	20%	No indication	No indication	12%	No indication	18.3%
Drive Spike - New	No indication	No indication	No indication	No indication	No indication	No indication	No indication
Drive Spike - Broken	No indication	37%	No indication	60%	100%	10%	12%
Drive Spike - Broken	No indication	45%	No indication	47%	100%	13%	20%
Drive Spike - Broken	No indication	57%	No indication	60%	100%	12%	17%

3.5 Discussion of Results

The surface roughness of the spike head affects the way sound interacts with the spike. With a flat surface, sound enters the material in a straight path using a flat transducer. However, the surface roughness of the head causes the sound to enter at an angle, creating refracted sound waves. It is more challenging to position the transducer correctly on the spike head to get an acceptable return signal.

As shown in [Figure 22a](#), a cut spike has a rounded head, and manufacturers put branding marks on the head of the spike making the surface less than ideal for transducers. A drive spike design has a protrusion on the head ([Figure 22b](#)). These protrusions can cause rocking of the transducer on the head of the spike, thus causing difficulties in getting stable contact between the transducer and the spike head. The square or rectangular drive spike head allows the inspector to move the transducer around the top of the spike. When installing a drive spike in a tie, the hammering forces can flatten the protrusions, slightly mitigating some of the roughness on the spike's head.

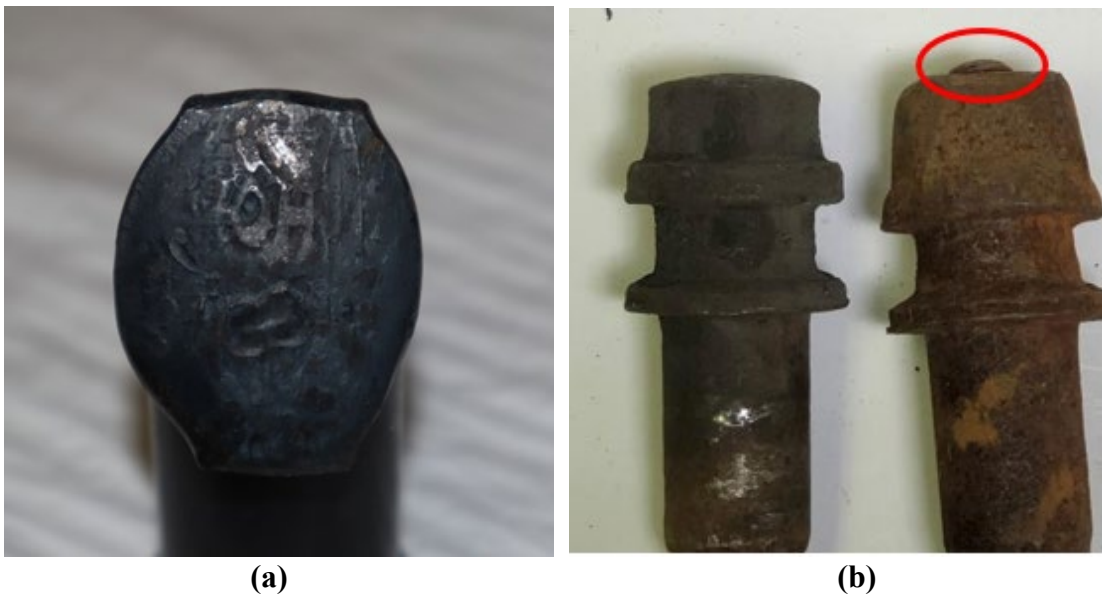


Figure 22. Spike surface conditions

As indicated by the laboratory test results, the orientation of the spike failure surface is a key factor to the signal reflection. The spikes with 10-degree and 20-degree EDM notches had weaker flaw indication compared to the spikes with 0-degree notches. The orientation could substantially affect the signal reflection. The input signal may never return to the transducers if the failure surface has a high orientation, resulting no signal indication for a broken spike.

[Figure 23](#) shows random samples of broken cut spikes from FAST. Unlike the EDM notch samples, the fracture surface is not developed on a perfectly flat plane. By visually comparing the failure surfaces to a 10-degree angle as indicated in [Figure 23](#), the failure planes were mostly below 10 degrees. This is an important observation in that it gives confidence that the UT method for spike detection may be successful. For example, spikes like Spike 4 had a failure surface close to 10 degrees or even higher. This may result in a missed report on these spikes. But since they represent a small portion of broken spikes, this detection method should be able to find most broken spikes and identify a broken spike issue for a specific section track.



Figure 23. Orientation of cut spike failure plane

4. In-track Ultrasonic Testing

TTCI performed in-track testing to evaluate the performance of selected transducers and investigate the effectiveness of the laboratory-developed UT procedure in the in-track condition. Based on the modeling and laboratory test results, three transducers were selected for in-track testing. This section summarizes test setup and results of the in-track testing for the following:

- 2.25-MHz, 0.5-inch diameter, single-element transducer
- 5-MHz, 0.5-inch diameter, single-element transducer
- 5-MHz, 0.5-inch diameter, 0-degree roof angle, dual-element transducer

4.1 Test Setup

To check the reliability of the UT procedure, a blind test zone was set up in a 6-degree curve on the HTL at FAST. The test zone included 10 cut spikes, 10 drive spikes, and 10 screw spikes. Each spike set included two broken spikes from track. Two spikes with a saw-cut notch were installed in the cut spike zone and the screw spike zone (two spikes of each zone). These spikes with saw-cut notches simulated a defective spike at a known depth along the spike shaft. Like the EDM notches used during the laboratory tests, the saw-cut notch was cut halfway through the spike shaft. [Table 7](#) lists the spike configuration of the test zone and spike condition of each spike.

Table 7. Spike condition for in-track blind test

Spike Type & Location	Actual Spike Condition	Spike Type and Location	Actual Spike Condition	Spike Type and Location	Actual Spike Condition
Cut Spike 1	Saw-cut notch at 3"	Drive Spike 1	Saw-cut notch at 4"	Screw Spike 1	Naturally broken
Cut Spike 2	Saw-cut notch at 3"	Drive Spike 2	Saw-cut notch at 4"	Screw Spike 2	Good
Cut Spike 3	Good	Drive Spike 3	Good	Screw Spike 3	Good
Cut Spike 4	Broken	Drive Spike 4	Naturally broken	Screw Spike 4	Naturally broken
Cut Spike 5	Good	Drive Spike 5	Naturally broken	Screw Spike 5	Good
Cut Spike 6	Good	Drive Spike 6	Good	Screw Spike 6	Good
Cut Spike 7	Good	Drive Spike 7	Good	Screw Spike	Good
Cut Spike 8	Broken	Drive Spike 8	Good	Screw Spike 8	Good
Cut Spike 9	Good	Drive Spike 9	Good	Screw Spike 9	Good
Cut Spike 10	Good	Drive Spike 10	Good	Screw Spike 10	Good

4.2 Test Results and Analysis

Similar to the laboratory testing, the percentage of signal amplitude for each detection was reported in the in-track testing. Tables 8, 9, and 110 presents the results of in-track UT testing. The detection error is summarized in Table 11. Based on the in-track testing data, Transducers 2, 4, and 5 can detect broken cut spikes. However, Transducers 2 and 4 failed to detect notched cut spikes accurately. Transducer 2 also reported a good cut spike as broken.

For the drive spikes Transducer 2 returned no indication for all spikes. Transducers 4 and 5 had Type I errors (no flaw was indicated where there was a flaw) and Type II errors (a flaw was indicated where there was no flaw). Even though all three transducers correctly detected broken screw spikes, they all had at least two Type I errors.

Table 8. In-track test results for cut spikes

Spike Type and Location	Actual Spike Condition	Transducer 2 2.25MHz, 0.5", single-element	Transducer 4 5MHz, 0.5", single-element	Transducer 5 5MHz, 0.5", dual-element
Cut Spike 1	Saw-cut notch at 3"	No indication	No indication	41%
Cut Spike 2	Saw-cut notch at 3"	90%	No indication	25%
Cut Spike 3	Good	No indication	No indication	No indication
Cut Spike 4	Broken	95%	29%	93%
Cut Spike 5	Good	No indication	No indication	No indication
Cut Spike 6	Good	No indication	No indication	No indication
Cut Spike 7	Good	No indication	No indication	No indication
Cut Spike 8	Broken	88%	34%	85%
Cut Spike 9	Good	No indication	No indication	No indication
Cut Spike 10	Good	42%	No indication	No indication

Table 9. In-track test results for drive spikes

Spike Type and Location	Actual Spike Condition	Transducer 2 2.25MHz, 0.5", single-element	Transducer 4 5MHz, 0.5", single-element	Transducer 5 5MHz, 0.5", dual-element
Drive Spike 1	Saw-cut notch at 4"	No indication	No indication	No indication
Drive Spike 2	Saw-cut notch at 4"	No indication	No indication	29%
Drive Spike 3	Good	No indication	No indication	21%
Drive Spike 4	Good	No indication	No indication	32%
Drive Spike 5	Broken	No indication	No indication	No indication
Drive Spike 6	Broken	No indication	30%	27%
Drive Spike 7	Good	No indication	No indication	No indication
Drive Spike 8	Good	No indication	No indication	No indication
Drive Spike 9	Good	No indication	35%	No indication
Drive Spike 10	Good	No indication	No indication	No indication

Table 10 In-track test results for screw spikes

Spike Type and Location	Actual Spike Condition	Transducer 2 2.25MHz, 0.5", single-element	Transducer 4 5MHz, 0.5", single-element	Transducer 5 5MHz, 0.5", dual-element
Screw Spike 1	Naturally broken	39%	100%	28%
Screw Spike 2	Good	No indication	No indication	32%
Screw Spike 3	Naturally broken	41%	35%	42%
Screw Spike 4	Good	35%	28%	No indication
Screw Spike 5	Good	70%	No indication	30%
Screw Spike 6	Good	50%	34%	No indication
Screw Spike 7	Good	No indication	No indication	No indication
Screw Spike 8	Good	No indication	No indication	No indication
Screw Spike 9	Good	No indication	No indication	No indication
Screw Spike 10	Good	No indication	No indication	No indication

Table 11. Summary of detection error for in-track testing

Type	Transducer 2	Transducer 4	Transducer 5
Cut Spike	Missed one notched spike. Reported a good spike as broken.	Missed two notched spikes.	No errors. All broken spikes detected.
Drive Spike	Missed two notched spikes. Missed two broken spikes.	Missed two notched spikes. Missed one broken spike. Reported a good spike as broken.	Missed one notched spike. Missed one broken spike. Reported two good spikes as broken.
Screw Spike	Reported three good spikes as broken.	Reported two good spikes as broken.	Reported two good spikes as broken.

The effect of head surface condition for drive spike detection was observed during laboratory testing. This effect was exacerbated during in-track testing because all drive spikes had surface protrusions at the spike head. Transducer positioning on these spikes was the biggest issue in the field condition. This may have been the primary cause for Type II errors.

As indicated in [Appendix B](#), the failure plane of drive and screw spikes was located where the threads started. Transducers picked up the signal return from the thread layers and this return was reported as a defect. In [Figure 24](#), the three red dots represent three signal peaks over 20 percent of the signal amplitude along the spike shaft. Two of them were within the depth range of interest (2.5 to 4 in.). The spike under test was a good screw spike but was reported broken. The signal return from the screw threads appeared to be the main source of Type I errors for drive and screw spikes.



Figure 24. Signal indication by thread layers

According to the in-track testing results, Transducers 4 and 5 gave the best results (clear indication and accurate defect reporting) for cut spike detection. None of the tested transducers detected drive and screw spike defects with a desirable success rate.

5. Conclusion

For this first phase of research, TTCI employed a multi-task approach to include ultrasonic beam modeling and simulation in spikes, laboratory testing on individual spikes with artificial defects, and blind UT testing of in-track spikes at the HTL, FAST.

The UT simulation was conducted for cut spikes and drive spikes. Different ultrasonic parameters, transducer frequencies, transducer sizes, and roof angles of dual-element transducers were evaluated in the simulation. The simulation results were used to characterize and optimize the ultrasonic inspection parameters. Simulation work showed that the frequency range of 5 MHz to 10 MHz generated acceptable signal reflection at the desired depth. Optimal transducer size was determined to be 0.5-inch diameter due to the limitation associated with the contact surface (head of the spike). Dual-element transducers with 0-degree roof angle gave the best signal reflection compared to dual-element transducers with higher roof angle values.

Next, researchers conducted laboratory testing to evaluate the effectiveness of the transducers as determined through a simulation approach for detecting breaks in actual spikes. First, they fabricated spike samples with machined (EDM) notches to simulate broken spike characteristics for controlled laboratory tests. Second, they developed a hand-held UT procedure and conducted tests to test spikes (cut spikes, drive spikes, and screw spikes) with EDM notches and broken spikes from track. Seven transducers with various specifications were used to inspect new spikes, EDM notched spikes, and broken spikes in the laboratory conditions. Three transducers generated acceptable signal reflection in the laboratory test. These include:

- 2.25-MHz, 0.5-inch diameter, single-element transducer
- 5-MHz, 0.5-inch diameter, single-element transducer
- 5-MHz, 0.5-inch diameter, 0-degree roof angle, dual-element transducer

Finally, TTCI conducted blind in-track testing at section 25 of the HTL, FAST, to evaluate the performance of selected transducers from laboratory testing and investigate the effectiveness of the laboratory-developed UT procedure for the in-track inspection. For this, 10 spikes of each spike type (cut spike, drive spike, screw spike) was set up on the HTL. Two transducers (5-MHz, 0.5-inch diameter, single-element and dual-element transducers) gave the best results (clear indication and accurate defect reporting) for *cut spike detection*. This finding also verified the simulation results since these two transducers were recommended by the modeling effort. However, none of the tested transducers could effectively detect defects in broken drive or screw spikes.

The simulation and testing in this study found that the orientation of the failure plane and the surface flatness of the spike head can notably affect the detection quality.

6. Future Research Recommendations

The objective of this research is to develop and test an automated method to detect broken spikes in wood-tie track.

TTCI envisions advancing this work in multiple phases. For the next phase of the work, researchers recommend the following:

1. Design and test a portable prototype NDE system capable of inspecting cut spikes based on the work conducted in Phase I.
2. Determine, optimize, and validate contact ultrasonic parameters for the drive spikes and screw spikes.
3. Determine an optimal transducer configuration and stand-off distance for an ultrasonic transducer for a non-contact UT approach.

7. References

- 1 Kerchof, B. (June 2017). A Derailment Investigation and Broken Spikes Presentation at the 2017 Wheel Rail Interaction Conference, Montreal.
- 2 Federal Railroad Administration (May 2019). Timber Crosstie Spike Fastener Failure Investigation [RR 19-14]. Washington, DC: U.S. Department of Transportation.
- 3 Gao, Y., McHenry, M., and Kerchof, B. (April 2018). Investigation of Broken Cut Spikes on Elastic Fastener Tie Plates Using an Integrated Simulation Method. *Proceedings, 2018 ASME/IEEE Joint Railroad Conference*, Pittsburgh.
- 4 Gao, Y. and McHenry, M. (June 2019). Modeling and Field Investigation of Spike Breakage on Elastic Fastener Tie Plates. Narvik, Norway.
- 5 Gao, Y., LoPresti, J. (April 2020). Interim Report: Broken Spike Remediation. *Technology Digest TD20-004*. Pueblo, CO: Association of American Railroads.
- 6 Gao, Y., Miller, M., and Williams, D. (June 2020). Field Investigation of Broken Cut Spikes on Elastic Fastener Plates: Revenue Service. *Technology Digest TD20-013*. Pueblo, CO: Association of American Railroads.
- 7 Deschamps, G. A. (1972). Ray Techniques in Electromagnetics. *Proceedings, IEEE, Vol. 60* (9), pp. 1022-1035.
- 8 Gengembre, N. and Lhémery, A. (2000). Pencil Method in Elastodynamics: Application to Ultrasonic Field Computation. *Ultrasonics*, 38 (1-8), 495-499.
- 9 CIVA NDE (2016). User Manual.
- 10 Mahaut, S., et al. (2009). Recent advances and current trends of ultrasonic modelling in CIVA. *Insight*, 51 (2).
- 11 Raillon, R. and Lecoœur-Taïbi, I. (2000). Transient Elastodynamic Model for Beam Defect Interaction: Application to Non-destructive Testing. *Ultrasonics*, 38 (1-8), 527-530.
- 12 Mahaut, S., et al. (2010). An overview of Ultrasonic beam propagation and flaw scattering models in the CIVA software. *AIP Conference Proceedings*, 1211, 2133-2140. DOI: <http://dx.doi.org/10.1063/1.3362393>.
- 13 Dorval, V., et al. (2015). Simulation of the UT Inspection of Planar Defects Using a Generic GTD-Kirchhoff Approach. *Proc. of 41st Annual Review of Progress in QNDE*, 1650 (1), 1750-1756. DOI:10.1063/1.4914798.
- 14 Krautkramer, J. and Krautkramer, H. (1990). *Ultrasonic Testing of Materials*. 4th revised edition, Springer Verlag.
- 15 Mason, W.J., and McSkimin, H.J. (1947). Attenuation and Scattering of High Frequency Sound Waves in Metals and Glasses. *J. Acoust. Soc. Am.*, 19, 464-473.
- 16 Ono, K. A. (2020). Comprehensive Report on Ultrasonic Attenuation of Engineering Materials, Including Metals, Ceramics, Polymers, Fiber-Reinforced Composites, Wood, and Rocks. *Appl. Sci.*, 10, 2230, 1-52.

Appendix A: Principles of Ultrasonic Testing and Ultrasonic Transducers

Principles of Ultrasonic Testing

UT is based on directing a sound wave signal to an object of interest and processing the received signal reflected from said object. The thickness (L) of a material, when measured using the pulse-echo ultrasonic method, is defined by the relation [14]:

$$L = \frac{v \times t}{2} \quad (1)$$

where, v is the velocity of sound in the material, and t is the transit time (round trip of ultrasound signal from the transmitter into the material and back to the receiver). The ultrasound wavelength λ in an isotropic material is directly related to the velocity of sound in a given material and frequency f and is generally expressed as [14]:

$$\lambda = \frac{v}{f} \quad (2)$$

The velocity of sound is not always the same. A sound is a form of a vibration of kinetic energy passing from molecule to molecule. The closer the molecules are to each other and the tighter their bonds, the less time it takes for them to pass the sound to each other and the faster sound can travel. For these reasons, the speed of sound is faster in solid materials and slower in liquids or gases. The speed of a sound wave is also affected by two properties of matter: the elastic properties and density. This relationship is best described by the following equation [14].

$$v = \sqrt{\frac{C_{ij}}{\rho}} \quad (3)$$

where, C_{ij} is the elastic properties and ρ is the density of the material.

In addition, the actual speed of the sound in materials may vary significantly due to specific composition or microstructure, grain or fiber orientation, porosity in materials, and ambient temperature. Generally, this is true in the case of cast metals, fiberglass, plastics, and composites.

Since the speed of sound propagation in the material is a function of material properties at given conditions and is independent of the amplitude, there is an inverse proportion of wavelength and frequency. The higher the frequency, the shorter the wavelength. In theory, a defect detection standard practice stipulates the *minimal size of the discontinuity to be at least one-half of the wavelength*. Resolution, therefore, increases with higher frequencies. This example holds for the ideal case when there is a single wave. In reality, the waves are emitted as short pulses or tone bursts and the focus is not to a single pinpoint. The waves propagate and even the defect with a lower size than one and one-half of the wavelength can be detected. However, the amplitude of the received signal is very low. Table A1 shows the estimated detectable flaw size in 1020 steel ($V_L = 5,900$ m/s and $V_s = 3,230$ m/s).

Table A1. Estimated detectable flaw size

Frequency MHz	$\lambda/2$ Longitudinal mm (in.)	$\lambda/2$ Transverse mm (in.)	$\lambda/2$ Surface mm (in.)
1	3.0 (0.12)	1.6 (0.06)	1.6 (0.06)
2.25	1.3 (0.05)	0.7 (0.03)	0.7 (0.03)
5	0.6 (0.02)	0.3 (0.01)	0.3 (0.01)
7.5	0.4 (0.02)	0.2 (0.01)	0.2 (0.01)
10	0.3 (0.01)	0.2 (0.01)	0.2 (0.01)
15	0.2 (0.01)	0.1 (0.004)	0.1 (0.004)
20	0.1 (0.01)	0.1 (0.003)	0.1 (0.003)
25	0.1 (0.01)	0.1 (0.003)	0.1 (0.002)

When ultrasonic waves travel in different media, they are reflected at boundaries where there exist differences in acoustical properties of the materials on each side of the boundary. This is usually referred to as the acoustic impedance mismatch. The acoustic impedance (Z) is defined by the relation [14]:

$$Z = \rho \times v \quad (4)$$

In general, the greater the impedance mismatch, the greater the percentage of energy that will be reflected at the interface or boundary between one medium and another. The amount of transmitted energy between two materials with acoustic impedances Z_1 and Z_2 is given by the transmission coefficient (T) [14]:

$$T = 1 - R = 1 - \left(\frac{Z_2 - Z_1}{Z_2 + Z_1} \right)^2 = \frac{4 Z_1 Z_2}{(Z_1 + Z_2)^2} \quad (5)$$

where, R is the reflection coefficient. This expression for T assumes that both couplant-material interfaces are acting independently and is only true for the normal incidence. For example, for a normal incidence of ultrasound, 88 percent of the ultrasonic energy is reflected at a water-steel interface. As the wave exits the part back through the front surface, only 1.3 percent of the original energy is transmitted back to the transducer (see Figure A1).

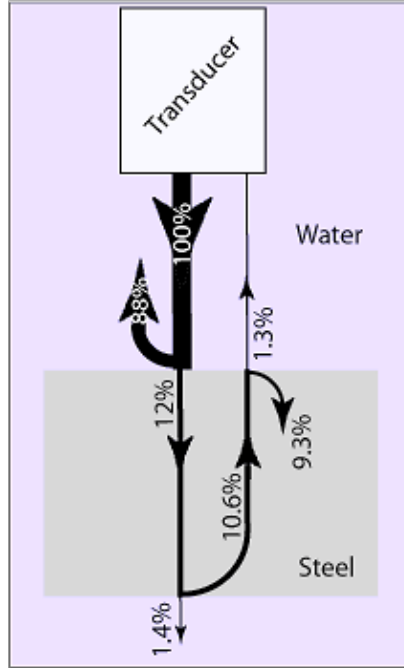


Figure A1. Transmission and reflection of ultrasonic energy in steel-water interface at normal incidence

[Photo credit](#)

The relative change in ultrasonic signal amplitude is commonly measured in decibels, the logarithmic value of the ratio of two signal amplitudes. The dB loss of energy on transmitting a signal from medium 1 into medium 2 with acoustic impedances Z_1 and Z_2 is given by the relation [14]:

$$dB\ loss_T = 10 \log_{10} \left[\frac{4 Z_1 Z_2}{(Z_1 + Z_2)^2} \right] \quad (6)$$

Similarly, the dB loss of energy of the ultrasonic signal in medium 1 reflecting from an interface boundary with medium 2 is given by [14]:

$$dB\ loss_R = 10 \log_{10} \left[\frac{(Z_2 - Z_1)^2}{(Z_1 + Z_2)^2} \right] \quad (7)$$

Considering these equations, the dB loss on transmitting from water ($Z = 1.48$) into 1020 steel ($Z = 45.41$) is about -9.13 dB; this also is the loss transmitting from 1020 steel into water. Similarly, the dB loss of the backwall echo in 1020 steel in water is -0.57 dB; this also is the dB loss of the echo off 1020 steel in water. Finally, assuming no major reflections, there are additional three causes of attenuation of ultrasonic signals: diffraction, absorption, and scattering.

Attenuation refers to the loss of ultrasound sound energy as the ultrasonic beam passes through the material. The amplitude (A) of ultrasonic wave in a sample decays and is expressed as [14]:

$$A = A_0 e^{-\alpha x} \quad (8)$$

where, A_0 is the reference (unattenuated) amplitude and α is the total attenuation coefficient after the wave propagates at a distance x from the initial location.

The coefficient α consists of three parts [14]:

$$\alpha = \alpha_G + \alpha_A + \alpha_S \quad (9)$$

In Equation 9, the first part α_G is related to geometrical spreading of the transducer field, the second part α_A is related to absorption, i.e., internal friction, and the third part α_S is related to scattering at the grain boundaries. In Equations 8 and 9, the attenuation coefficients have the dimension 1/length, usually mm^{-1} . The factor to convert dB/mm into mm^{-1} is 8.686, i.e., the unit dB/mm divided by 8.686 corresponds to mm^{-1} . Moreover, ultrasonic energy loss due to absorption is a result of mechanisms such as dislocation, damping, hysteresis losses, thermoelastic effects. Similarly, loss due to scattering in polycrystalline materials depends on the ratio of grain size (D) and wavelength (λ). Rayleigh scattering depends on the fourth power of frequency, f^4 , that arises from random scattering centers, such as grain boundaries and distributed second phase particles [15]. This occurs when the distance between scattering centers, d , is much less than λ , or $\lambda \gg d$ [16]. Therefore, the amount of attenuation through a material can play an important role in the selection of a transducer for an application.

It is also important to understand the characteristic of an ultrasonic beam field radiated by an ultrasonic transducer. The beam field for any given ultrasonic transducer is divided into two zones: the near field and the far field. The near field is the region directly in front of the transducer where the echo amplitude goes through a series of maxima and minima and ends at the last maximum, at distance N from the transducer. Figure A2 shows the schematic of the ultrasonic beam field.

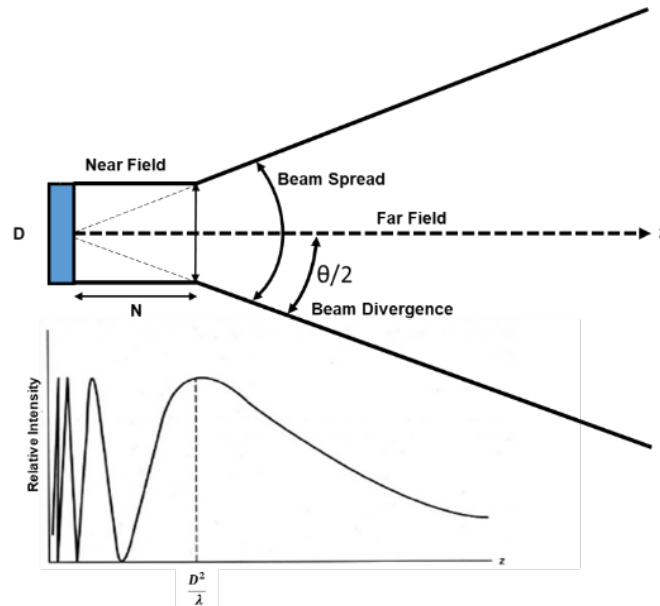


Figure A2. Transducer near and far field

The location of the last maximum is known as the near field distance (N), or Fresnel zone, and is the natural focus of the transducer. The far field, or the Fraunhofer zone, is the area beyond N where the sound field pressure gradually drops to zero. Because of the variations within the near field, it can be difficult to accurately evaluate flaws using amplitude-based techniques.

The near field distance is a function of the transducer element diameter (D), and wavelength (λ) and is expressed as [14]:

$$N = \frac{D^2}{4\lambda} \quad (10)$$

An ultrasonic beam spreads out or diverges after a certain point along its transmission axis as it travels through a medium. This phenomenon is usually referred to as beam spread but is sometimes also referred to as beam divergence or ultrasonic diffraction. Note that there is a difference between beam spread and beam divergence. Beam spread is a measure of the whole angle from side-to-side of the main lobe of the sound beam in the far field. Beam divergence is a measure of the angle from one side of the sound beam to the central axis of the beam in the far field. Therefore, beam spread is twice the beam divergence. Beam spread occurs because the vibrating particle of the material (through which the wave is traveling) do not always transfer all of their energy in the direction of wave propagation. For a flat piston source transducer, the beam spread is largely determined by the frequency and diameter of the transducer and is expressed as [14]:

$$\sin \theta/2 = 1.2 \frac{\lambda}{D} = 1.2 \frac{v}{Df} \quad (11)$$

where, $\theta/2$ is the beam divergence angle from centerline to point where signal is at half strength.

Ultrasonic Transducers

An ultrasonic transducer is a device that converts electrical energy to mechanical energy in the form of sound (mechanical wave), and vice versa. An active element inside the transducer is responsible in generating sound waves. The active element is basically a piece of polarized material (i.e., some parts of the molecule are positively charged, while other parts of the molecule are negatively charged) with electrodes attached to two of its opposite faces. When an electric field is applied across the material, the polarized molecules align themselves with the electric field, resulting in induced dipoles within the molecular or crystal structure of the material. This alignment of molecules will cause the material to change dimensions. This phenomenon is known as electrostriction. In addition, a permanently polarized material such as quartz (SiO_2) or barium titanate (BaTiO_3) will produce an electric field when the material changes dimensions because of an imposed mechanical force. This phenomenon is known as the piezoelectric effect.

The active element of most acoustic transducers used today is a piezoelectric ceramic, which can be cut in various ways to produce different wave modes (X-cut generates L-wave, and Y-cut produces S-wave modes). The thickness of the active element is determined by the desired frequency of the transducer. A wafer-thin element vibrates with a wavelength that is twice its thickness. Therefore, piezoelectric crystals are cut to a thickness that is one-half the desired radiated wavelength. The higher the frequency of the transducer, the thinner the active element. To get as much energy out of the transducer as possible, an impedance matching is placed between the active element and the face of the transducer. Optimal impedance matching is achieved by sizing the matching layer so that its thickness is one-quarter of the desired wavelength. This keeps waves that were reflected within the matching layer in phase when they

exit the layer. For contact transducers, the matching layer is made from a material that has an acoustical impedance between the active element and steel. Immersion transducers have a matching layer with an acoustical impedance between the active element and water. Contact transducers also incorporate a wear plate to protect the matching layer and active element from scratching. Finally, the backing material supporting the crystal has a great influence on the damping characteristics of a transducer. Using a backing material with an impedance like that of the active element will produce the most effective damping. Such a transducer will have a wider bandwidth, resulting in higher sensitivity. As the mismatch in impedance between the active element and the backing material increases, material penetration increases but transducer sensitivity is reduced. [Figure A3](#) shows the illustration of transducer and its elements.

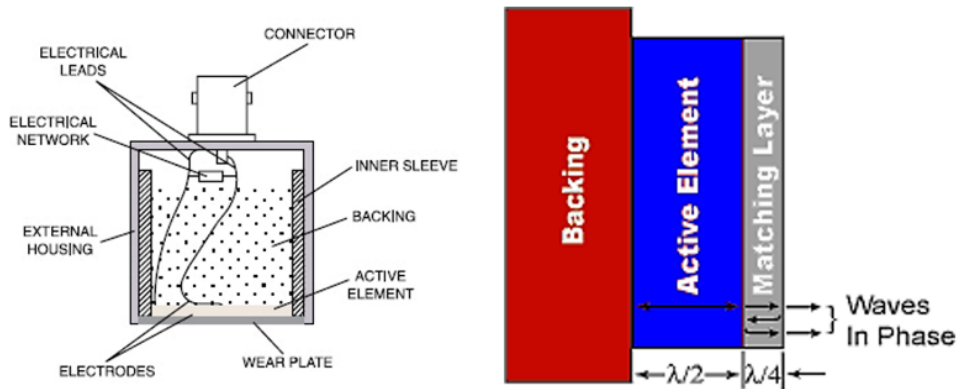


Figure A3. Schematic of ultrasonic transducer

[Photo credit](#)

Unlike single-element transducers, a dual-element transducer has two independent crystal elements housed in the same case, separated by an acoustic barrier. One of the elements transmits longitudinal waves while the other acts as a receiver. These elements are angled toward each other to create a V-shaped sound path in the test material. This pseudo-focus enhances the resolution in the focal zone. These transducers are typically designed for excellent near-surface resolution, good coupling to rough surfaces, and reduced back-scattering noise in coarse-grained or scattering materials while maintaining high sensitivity. They are used primarily for flaw detection and thickness gauging. [Figure A4](#) is a schematic of a typical dual-element probe.

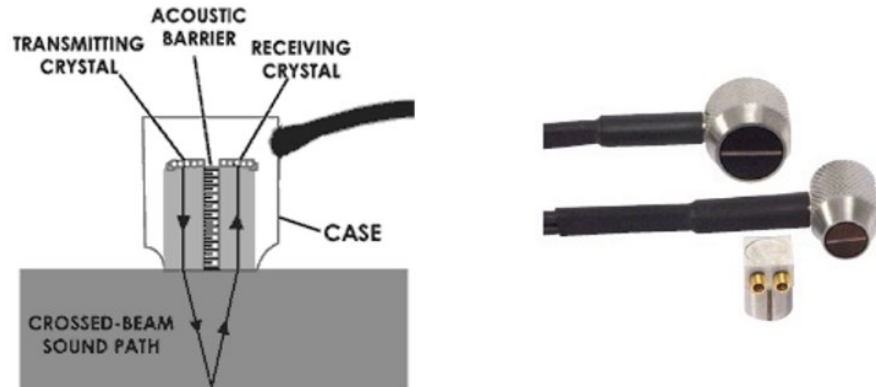


Figure A4. Dual-element transducer: (a) schematic of the probe showing two elements and sound path and (b) examples of different types of dual-element transducers

[Photo credit](#)

It is also possible to achieve a very long range (equal to single element) when the roof angle is set to close to 0 degree. But then the ability to detect a small indication close to the surface may be compromised due to the weak sound field between the transmitting and receiving elements directly below the probe. In general, a decrease in the roof angle or an increase in the transducer element size will result in a longer pseudo-focal distance and an increase in a useful range.

Appendix B: Spike Failure Plane Locations

Figure B1 presents the failure plane locations on broken spikes of different spike types. The samples were selected from FAST. The measurement was the distance between the top of the spike (also the contact surface of UT transducer and spike) and the failure plane. Cut spikes were from an anchor spike location and typically broke at 2.5 to 3.5 inches; most drive/screw spikes broke at 3.0 to 4.0 inches – where the threaded portion starts. According to different designs of screw spikes, the threaded portion starts at different locations. For example, the thread portion of the last spike in Figure B1 initiated at 3 inches.



Figure B1. Failure plane locations on broken spikes of different spike types from FAST

Figure B2 shows two, half-broken spikes (rail spike location) found in revenue service track. The failure locations were deeper than the cut spikes in an anchor spike location at FAST, which were at 3.4 and 3.9 inches, respectively.



Figure B2. Failure plane locations on cut spikes (rail spike location) from revenue service

The spike failure planes generally fell in a range of 2.5 to 4.0 inches from the top of the spike head. The UT simulation uses this data to evaluate the coverage of beam field, and the UT testing will use this depth range as a guide to identify the defects in in-track spikes.

Abbreviations and Acronyms

FRA	Federal Railroad Administration
TTCI	Transportation Technology Center, Inc.
TTC	Transportation Technology Center
FAST	Facility for Accelerated Service Testing
HTL	High Tonnage Loop
EDM	Electro-Discharged Machining
NDE	Non-Destructive Evaluation
UT	Ultrasonic Testing
GTD	Geometrical Theory of Diffraction
SOV	Separation of Variables
DF	Detailed Fracture